The membrane insertion of the pro-apoptotic protein Bax is a Tom22-dependent multi-step process: a study in nanodiscs

Akandé Rouchidane Eyitayo[1], Laetitia Daury[2], Muriel Priault[1], Stéphen Manon[1,3]

[1]CNRS, Université de Bordeaux, UMR 5095, IBGC, Bordeaux, France

[2]CNRS, Université de Bordeaux, UMR 5248, CBMN, Pessac, France

[3]Corresponding author: manon@ibgc.cnrs.fr

Abstract

Bax membrane insertion was investigated by setting up cell-free synthesis of Bax in the presence of pre-formed nanodiscs. While Bax was not spontaneously inserted in nanodiscs, co-synthesis with the mitochondrial receptor Tom22 promoted Bax membrane insertion. The initial interaction of Bax with the lipid bilayer exposed the hydrophobic GALLL motif in Hα1 leading to Bax precipitation through hydrophobic interactions. The same motif was recognized by Tom22, triggering conformational changes leading to the extrusion, then the membrane insertion of the C-terminal hydrophobic Hα9. This was impaired by a $D^{154}Y$ substitution in Hα7, that is found in some tumors. Conversely, a $R^{9}E$ substitution promoted the spontaneous insertion of Bax in nanodiscs, thus recapitulating the action of Tom22. Both Tom22-activated Bax and Bax$R^{9}E$ alone permeabilized liposomes to dextran-10kDa and formed ~5nm-diameter pores in nanodiscs. Tom22 was required for Bax-membrane insertion following its engagement with Bcl-xL, then release by a BH3-mimetic. The concerted regulation of Bax membrane insertion by Tom22 and BH3-activators is discussed.

Introduction

The mitochondrial pathway of apoptosis involves proteins of the Bcl-2 family, including anti-apoptotic proteins, such as Bcl-2 and Bcl-xL, multi-domain pro-apoptotic proteins Bax, Bak and Bok, and pro-apoptotic BH3-only proteins, such as Bid and Bim (Green, 2022; Czabotar and García-Saez, 2023; for recent reviews). The most abundant Bcl-2 family member in healthy cells (Simonyan et al., 2023), Bax is inactive in the cytosol or loosely bound to intracellular membranes. It becomes active following apoptotic signals that induce a series of events, including its relocation to the mitochondrial outer membrane (MOM) (Wolter et al., 1997), rupture from inhibiting interactions with anti-apoptotic proteins (Sedlak et al., 1995), conformational changes induced by BH3-only proteins (Desagher et al., 1999; Marani et al., 2002), MOM-insertion (Goping et al., 1998), oligomerization (Antonsson et al., 2000), then culminating in the formation of a pore that permeabilizes MOM to apoptogenic factors (Schlesinger et al., 1997; Pavlov et al., 2001). Although there is a large consensus about the nature of these events, their sequence and relative importance in the control of Bax-induced MOM-permeabilization is still debated and are the focus of ongoing investigations.

Soluble, inactive Bax is structured in 9 α-helices, organized around a hairpin formed by Hα5 and Hα6 (Suzuki et al., 2000). The C-terminal Hα9 is hydrophobic, like the C-terminal membrane anchors of anti-apoptotic proteins Bcl-2 and Bcl-xL (Wolter et al., 1997; Kaufmann et al., 2003). However, Bax-Hα9 does not drive the MOM-insertion of Bcl-xL while the C-terminal α-helix of Bcl-xL drives the MOM-insertion of Bax (Tremblais et al., 1999; Suzuki et al., 2000). Indeed, Bax Hα9 is stabilized in a hydrophobic groove formed by the BH domains, owing to the presence of hydrophobic residues on its core-facing side and hydroxyl residues on its outside-facing side (Suzuki et al., 2000). The only hydroxyl residue on the core-facing side, S^{184}, is stabilized by a hydrogen bond with D^{98} in Hα4. The deletion of S^{184}, or its substitution by a non-hydroxylated residue, promotes the spontaneous insertion of Bax in both reconstituted and cellular models (Suzuki et al., 2000; Arokium et al., 2007; Cartron et al., 2008; Kale et al., 2018). The extrusion of Hα9 from the hydrophobic groove thus appears as a crucial step towards Bax membrane-insertion.

Because of the stability of the D^{98}/S^{184} hydrogen bond, it is unlikely that another BH3 domain would be able to displace Hα9 from the hydrophobic groove, unless a previous conformational change weakening this bond had previously occurred (Suzuki et al., 2000). Interestingly, the BH3-only protein Bim binds at a site close to Hα1, α1-α2 loop and Hα6 ("non-canonical" binding site) (Gavathiotis et al., 2008), resulting in long-range conformational changes that may ultimately lead to the extrusion and the

insertion of Hα9 (Gavathiotis et al., 2010). Mutagenesis-induced conformational changes in the α1-α2 loop actually promoted Hα9 extrusion (Dengler et al., 2021). Anti-apoptotic proteins competing with Bim-binding (Barclay et al., 2015), or mutations in Bax (Garner et al., 2017) might block these conformational changes.

The N-terminal extremity of Bax is also involved in the regulation of its mitochondrial localization. Indeed, the deletion of the 19 N-terminal residues generates a variant having a constitutive mitochondrial localization (Goping et al., 1998). A similar Bax variant, called BaxΨ, was found in low grade glioblastomas displaying high level of apoptosis (Cartron et al., 2002). Bax-Hα1 (residues 16-35) fused to RFP competed with the mitochondrial addressing of BaxΨ, suggesting that a receptor for Hα1 was involved in Bax mitochondrial localization (Cartron et al., 2003). Hα1 was further shown to interact with the mitochondrial receptor Tom22, a component of the TOM complex (Translocase of Outer Membrane) (Bellot et al., 2007). The down-regulation of Tom22 decreased Bax mitochondrial localization in apoptotic mammalian cells (Bellot et al., 2007; Cartron et al., 2008) and following heterologous expression in yeast (Bellot et al., 2007; Ott et al., 2007) and in *Drosophila* (Colin et al., 2009). However, because other studies did not report any significant role of TOM components on Bax localization in mammalian cells (Ross et al., 2009) nor in yeast (Sanjuán-Szklarz et al., 2007), the potential role of Tom22 in Bax mitochondrial localization remains debated. It has also been shown that another TOM subunit, namely Tom20, was involved in the mitochondrial localization of Bcl-2 (Motz et al., 2002; Lalier et al., 2021) and that Metaxins 1 and 2, components of the SAM complex (Sorting and Assembly Machinery), were involved in the mitochondrial localization and activation of Bak (Cartron et al., 2014; Petit et al., 2017), in addition to VDAC2 (Cheng et al., 2003). VDAC2 might also be involved in the regulation of Bax localization and activation (Ma et al., 2014; Lauterwasser et al., 2016). It therefore appears that the role of MOM proteins in the targeting, activation and regulation of Bcl-2 family members might have been somewhat overlooked and thus requires further investigations (Ott et al., 2009; Yuan et al., 2021; Lalier et al., 2022; for reviews).

The reconstitution of membrane proteins in nanodiscs, associated to cryoEM, is a successful approach not only to resolve the structure of membrane proteins but also to gain insight into mechanistic aspects (Thonghin et al., 2018; García-Nafría and Tate, 2021; Notti and Walz, 2022; for reviews). A cryoEM study of Bax activated by Bid-BH3 at low pH, and co-formed with nanodiscs, showed the occurrence of a small pore (~3.5nm in diameter) (Xu et al., 2013). On this basis, molecular dynamics approaches led to a model of a lipidic pore generated by the reorganization of a limited number of lipid molecules

around Bax (López et al., 2019). We have recently set-up a more direct approach by combining the cell-free synthesis of Bax and its direct insertion into pre-formed nanodiscs (Rouchidane Eyitayo et al., 2023a). We used BaxWT and a mutant BaxP^{168}A, that had been previously shown to be spontaneously membrane-inserted in glioblastoma cells (Cartron et al., 2005), yeast cells (Arokium et al., 2004) and liposomes (Simonyan et al., 2017). While both variants were soluble when synthesized in the absence of nanodiscs, they were partially precipitated in the presence of nanodiscs and were not inserted (Rouchidane Eyitayo et al., 2023a). The precipitated fraction, that contained pure Bax, was solubilized in Brij-58 and used to co-form nanodiscs: interestingly, nanodiscs containing BaxP^{168}A displayed a larger size than those containing BaxWT, and some of them displayed a pore having a diameter close to 5nm (Rouchidane Eyitayo et al, 2023a). However, the objects were heterogeneous, precluding further structural investigations. Subsequently, we observed that the cell-free co-synthesis of Bax with its anti-apoptotic partner Bcl-xL induced the spontaneous co-insertion of both proteins into nanodiscs, likely under the form of an inactive heterodimer (Rouchidane Eyitayo et al., 2003b).

These data urged us to further investigate the mechanisms underlying Bax interaction with nanodiscs and the possible role of Tom22, by setting-up a minimal system involving the co-synthesis of Bax and Tom22 in the presence of nanodiscs. By using several Bax mutants, we show that Tom22 interacts with Bax Hα1 to promote a conformational change resulting in the extrusion and the insertion of Bax Hα9. Furthermore, Tom22 promoted the ability of Bax to form a pore in nanodiscs and liposomes, and was required for Bax-membrane insertion following Bax priming by its engagement with Bcl-xL then release by the BH3-mimetic WEHI-539. We propose a model that emphasizes the concerted action of Tom22 and BH3-activators in Bax targeting, insertion and pore formation.

Results

The co-synthesis of Tom22 prevents Bax precipitation and stimulates Bax insertion into nanodiscs

The cell-free synthesis of Bax was coupled to its direct insertion into pre-formed nanodiscs (Rouchidane Eyitayo et al., 2023ab). We observed that the presence of nanodiscs induced the precipitation of a large fraction of Bax, while nanodiscs remained in the supernatant (Rouchidane Eyitayo et al., 2023a) (Fig.1A). We then checked if the fraction of Bax remaining in the supernatant was associated or not to nanodiscs. Nanodiscs were bound to Ni-NTA-sepharose and the presence of Bax was measured in the unbound and bound fractions. The vast majority of Bax remained in the unbound fraction, therefore not associated to nanodiscs (Fig.1C).

It has been reported that the mitochondrial receptor Tom22 was involved in Bax targeting to the MOM (Bellot et al., 2007). We then tested the effect of the co-synthesis of Tom22 with Bax and observed that it prevented Bax precipitation (Fig.1AB) and promoted the association of Bax to nanodiscs (Fig.1CD). Nanodiscs were then submitted to an alkaline treatment to remove peripheral proteins. We first verified that the treatment did not alter the stability of nanodiscs (Fig.S1A) and efficiently removed Kras, a known peripheral protein (Lee et al., 2023) (Fig.S1B). Contrary to Kras, a large fraction of Bax remained associated to nanodiscs, showing that the co-synthesis of Tom22 actually promoted the membrane insertion of Bax (Fig.1E).

The alkaline treatment showed that Tom22 was itself inserted into nanodiscs (Fig.1E). We have reported that the stimulation of Bax insertion in nanodiscs by the co-synthesis of Bcl-xL depended on the insertion of Bcl-xL: indeed, Bcl-xLΔC, deprived of the C-terminal membrane anchor (Kaufmann et al., 2003), did not stimulate Bax insertion into nanodiscs (Rouchidane Eyitayo et al., 2023b). We then asked whether the insertion of Tom22 was required or not for Bax insertion into nanodiscs. Bax was co-synthesized with the cytosolic N-terminal domain of Tom22 (residues 1-52), that contains the negatively charged residues involved in the recognition of mitochondria-targeted proteins (Nargang et al., 1998). Tom22(1-52) had the same effect as full-length Tom22 on the prevention of Bax precipitation (Fig.1F), on Bax association to nanodiscs (Fig.1DG) and on Bax insertion (Fig.1H). We concluded that, contrary to Bcl-xL, the membrane insertion of Tom22 was not required to promote Bax insertion. This showed that the stimulating effect of Tom22 on Bax insertion did not involve the co-insertion of the two proteins, but rather initiated a conformational change of Bax enabling its membrane insertion.

Bax precipitation and Tom22 effects depend on the exposure of the hydrophobic GALLL motif in Bax Hα1

The interaction of soluble Bax with liposomes induces the exposure of the N-terminal epitope recognized by the 6A7 antibody (Yethon et al., 2003), that is masked in soluble, inactive Bax (Hsu and Youle, 1997). We then tested if nanodiscs had the same effect as liposomes. Bax was synthesized in the absence of nanodiscs, then added to nanodiscs: their presence significantly increased the exposure of the 6A7 epitope, up to the same level as the constitutively active mutant Bax$R^{9}E$ (Arokium et al., 2007; see also below) in which the 6A7 epitope was constitutively exposed (Fig.2A). This antibody recognizes residues ^{13}PTSSEQI^{19} of Bax only when they move away from the core of the protein

(Peyerl et al., 2007). This epitope is located within the ART sequence (Apoptotic Regulation of Targeting; residues 1-19), of which the full deletion stimulates Bax mitochondrial localization and its ability to release cytochrome c (Goping et al., 1998; Cartron et al., 2003). The naturally occurring variant BaxΨ, carrying the same deletion, was found in low grade glioblastomas exhibiting a high level of apoptosis (Cartron et al., 2002).

We tested the hypothesis that the interaction of Bax with nanodiscs induced a movement of ART resulting in the exposure of hydrophobic domains leading to Bax precipitation, by comparing the cell-free synthesis of full-length Bax (BaxWT) and BaxΨ, in the absence or the presence of nanodiscs. BaxΨ precipitated even in the absence of nanodiscs (Fig.2B), suggesting that the precipitation of full-length BaxWT in the presence of nanodiscs might be related to a movement of ART. As expected, when synthesized in the presence of nanodiscs, BaxΨ also precipitated (Fig.2B) and the small fraction remaining in the supernatant was not inserted (Fig.2C). When co-synthesized with Tom22, the vast majority of BaxΨ was found in the supernatant (compare Fig.2D and Fig.2B), and a significant fraction was inserted in nanodiscs (Fig.2E). These data showed that, like for full-length BaxWT, the membrane-insertion of BaxΨ was rescued by the co-synthesis of Tom22.

ART deletion exposes Hα1, and substitutions in this helix decrease the mitochondrial localization of both BaxΨ and BaxWT (Cartron et al., 2003). Hα1 contains a succession of hydrophilic and hydrophobic residues, with a longer motif of five hydrophobic residues ^{23}GALLL^{27}, thus displaying a hydrophobic face, and a hydrophilic face that is interrupted by a hydrophobic helix turn (Fig.2F). We therefore tested the hypothesis that the exposure of the hydrophobic GALLL motif was responsible for Bax precipitation by replacing A^{24} or L^{26} by hydrophilic residues R and Q, respectively. Contrary to BaxWT, mutants BaxA^{24}R and BaxL^{26}Q did not precipitate when they were synthesized in the presence of nanodiscs (Fig.2G), showing that the hydrophobic GALLL motif was indeed responsible for Bax precipitation once Hα1 has been exposed. However, when co-expressed with Tom22, BaxA^{24}R was not inserted (Fig.2H), emphasizing the role of the GALLL motif in Bax/Tom22 interaction, in agreement with the observation that Tom22 binds to GALLL-containing peptides (Bellot et al., 2007). The mutant L^{26}Q displayed an intermediate behavior between wild-type Tom22 and the mutant A^{24}R (Fig.S2).

In cellulo, the interaction between Bax and Tom22 only occurred after apoptosis had been triggered, suggesting that an initial conformational change of Bax, induced by an apoptotic signal, was required (Bellot et al., 2007). We therefore tested the effect of BH3 activators, which promote Bax membrane insertion on isolated mitochondria and liposomes: we observed that cBid, Bid-BH3 and Bim-BH3

peptides and the Bim-BH3 analog BSTA1 did not prevent nanodisc-induced Bax precipitation (Fig.S3AB) and did nor stimulate Bax insertion (Fig.S3CD). However, the co-synthesis of Tom22 prevented Bax precipitation and restored Bax insertion in the presence of BH3 activators (Fig.S3EF).

Importantly, the effects of Tom22 were specific: the co-synthesis of Bax with Tom20, another receptor of the TOM complex, did not prevent Bax precipitation nor promote Bax insertion (Fig.S4AB). This is consistent with the observation that the down-regulation of Tom20 did not change Bax mitochondrial localization and function *in cellulo* (Bellot et al., 2007).

Taken altogether, these data suggested that a two-step process initiated Bax insertion into nanodiscs: (i) the interaction of Bax with the lipid bilayer induced a movement of ART that exposed the GALLL motif in Hα1 and (ii) Tom22 interacted with the GALLL motif, thus triggering conformational changes leading to Bax membrane insertion. We next investigated the nature of these conformational changes.

Tom22 triggers a conformational change leading to the extrusion of Bax Hα9

Because the stability of the soluble conformation of Bax depends on the engagement of its C-terminal hydrophobic Hα9 in the hydrophobic groove, Bax insertion first requires the extrusion of Hα9 from the groove (Suzuki et al., 2000). To investigate the effect of Tom22 on Hα9, we measured the exposure of a single cysteine residue introduced at position 177. We first verified that a triple mutant Bax$C^{62}S/C^{126}S/V^{177}C$ behave like BaxWT: as expected, it was not inserted into nanodiscs in the absence of Tom22 and was inserted in the presence of Tom22 (Fig.3A). We next measured the exposure of the $V^{177}C$ residue in the different fractions through the binding of NEM-PEG (Fig.3B). In the absence of nanodiscs, $V^{177}C$ was accessible to NEM-PEG. When synthesized in the presence of nanodiscs, $V^{177}C$ residue of the soluble fraction of Bax remained exposed, independently from the co-synthesis of Tom22. On the contrary, $V^{177}C$ of nanodisc-inserted Bax (in the presence of Tom22) was no longer accessible, showing that Hα9 was inserted into the lipid bilayer.

We next asked if the insertion of Hα9 was a prerequisite for Tom22-induced membrane-insertion of Bax, and the protection against nanodisc-induced precipitation. For this, we measured the behavior of Bax deprived of Hα9 (BaxΔα9, residues 1-169). Like full-length BaxWT, and contrary to BaxΨ, BaxΔα9 was soluble in the absence of nanodiscs and precipitated in their presence (Fig.3C). However, its precipitation was not prevented by the co-synthesis with Tom22 (Fig.3C). As expected, BaxΔα9 was not inserted in nanodiscs (Fig.3D). These data confirmed that the rescue of Bax precipitation by Tom22 was actually related to the Hα9-dependent insertion of Bax.

To discard the possibility that a side effect linked to the full deletion of Hα9 was responsible for nanodisc-induced Bax precipitation, we constructed a mutant carrying a single $T^{174}P$ substitution in this helix, thus keeping its length, but breaking its helical conformation. According to the Cosmic database (https://cancer.sanger.ac.uk/cosmic), this substitution is frequently found in squamous cell carcinomas of the upper digestive track (Martin et al., 2014). We found that the co-synthesis of Tom22 did not significantly rescue the precipitation of $BaxT^{174}P$ (Fig.3E) and did not stimulate its membrane-insertion (Fig.3F).

These data established that the presence of a Hα9 able to insert into the bilayer, was required for the effects of Tom22 both on the prevention of Bax precipitation, and the stimulation of Bax insertion into nanodiscs. This is consistent with a model where, following the initial interaction of Bax with the lipid bilayer exposing the GALLL motif of Hα1, without any conformational change at the C-terminus, the subsequent interaction of Tom22 with the GALLL motif promoted the extrusion of Hα9 followed by its insertion. This later step could not occur in BaxΔα9 and $BaxT^{174}P$ mutants, resulting in their precipitation caused by the hydrophobic interaction between GALLL motifs.

Involvement of D^{154} in the Tom22-mediated conformational change of Bax

We have reported that soluble, inactive Bax might be stabilized by an electrostatic interaction between residue R^9 in the ART and residue D^{154} in Hα7: indeed, single charge inversions of either one of these residues (R^9E or $D^{154}K$) resulted in their constitutive mitochondrial localization and permeabilization of the MOM to cytochrome c, while the double-substituted mutant $R^9E/D^{154}K$, in which the electrostatic interaction is restored, displayed the same soluble, inactive conformation as BaxWT (Arokium et al., 2007). We then investigated a possible role of these residues on the effects of Tom22.

The presence of a $D^{154}Y$ substitution in some tumors has been reported in Uniprot (https://www.uniprot.org/uniprotkb/Q07812/variant-viewer) and in the Spanish database Intogen (https://www.intogen.org/search?gene=BAX). Like for BaxWT, the co-synthesis of Tom22 protected $BaxD^{154}Y$ against nanodisc-induced precipitation (Fig.4A). However, contrary to BaxWT, Tom22 did not promote $BaxD^{154}Y$ insertion (Fig.4B). From these data, we concluded that the substitution $D^{154}Y$ did not impair the interaction of Bax with Tom22 and the associated rescue of Bax precipitation, but rather prevented Tom22-induced conformational change leading to Bax insertion.

The R^9E mutation of Bax mimics the effects of Tom22

As cited above, the electrostatic interaction between D^{154} and R^{9} might be involved in the stability of soluble, inactive Bax (Arokium et al., 2007). We therefore tested the effect of the mutation $R^{9}E$ and of the double mutation $R^{9}E/D^{154}K$ on Bax precipitation. Contrary to BaxWT, Bax$R^{9}E$ did not precipitate when synthesized in the presence of nanodiscs (Fig.4C) and was spontaneously associated to nanodiscs (Fig.4D). As expected, this was reversed by the introduction of the $D^{154}K$ mutation (Fig.4CD).

We next tested if the $R^{9}E$ substitution actually induced the spontaneous insertion of Hα9 in nanodiscs. The $R^{9}E$ substitution was introduced in the triple mutant Bax$C^{62}S/C^{126}S/V^{177}C$ described above. NEM-PEG labeling was done on nanodisc-bound and unbound fractions. While the unbound fraction contained labeled Bax, the nanodisc-bound fraction did not, showing that Hα9 was actually inserted in the lipid bilayer (Fig.4E). We then tested if the insertion of Hα9 was required for the protective effect of the $R^{9}E$ substitution on nanodisc-induced precipitation. A Bax$R^{9}E$/Δα9 mutant was constructed, and we observed that the deletion of Hα9 impaired the protective effect of the $R^{9}E$ mutation on Bax precipitation (Fig.4F). As expected, except for a faint band, the BaxR9E/Δα9 mutant was not associated to nanodiscs (Fig.4G). These data showed that the Bax$R^{9}E$ mutant synthesized alone displayed the same behavior as BaxWT co-synthesized with Tom22, and thus fully recapitulated the conformational changes initiated by the interaction of Bax with Tom22, leading to the insertion of Hα9.

Functional properties of Bax inserted through Tom22-mediated conformational change

We then investigated if Bax was active when its insertion was stimulated by the co-synthesis with Tom22. Cell-free synthesis was done in the presence of liposomes loaded with Dextran-FITC (10kDa). An anti-FITC antibody was added to quench the fluorescence of released Dextran-FITC, and the fluorescence decay was followed during the co-synthesis of Bax and Tom22(1-52). BaxWT and Bax$R^{9}E$ were synthesized alone in parallel. The co-synthesis with Tom22(1-52) increased the rate of fluorescence decay induced by BaxWT (Fig.5AB). This suggested that Tom22(1-52) not only stimulated the insertion of BaxWT but further stimulated its ability to form pores permeable to a molecule having a similar size as cytochrome c (12.5kDa). Interestingly, Bax$R^{9}E$ synthesized alone without Tom22 also exhibited a higher rate of permeabilization, consistent with the above experiments showing that it recapitulated the effect of Tom22. These experiments suggested that both BaxWT co-synthesized with Tom22(1-52) and Bax$R^{9}E$ synthesized alone were able to form pores large enough to release cytochrome c.

We then did TEM observations of negatively stained nanodiscs. Both Bax/Tom22(1-52) and Bax$R^{9}E$

could form nanodiscs having a structure resembling a pore (Fig.5C) with a diameter of about 5 nm (Fig.5DE). This was consistent with both electrophysiology experiments on MOM (Dejean et al., 2005; Guihard et al., 2004) and reconstituted oligomers (Dejean et al., 2005), and with TEM observations of precipitated/resolubilized oligomers of BaxP^{168}A reconstituted in nanodiscs by the co-formation method (Rouchidane Eyitayo et al., 2023a). These data showed that the direct nanodisc insertion of BaxWT co-synthesized with Tom22 as well as that of BaxR^{9}E synthesized alone accurately embodied the apoptotic pore.

In cancer cells, the overexpression of anti-apoptotic proteins, such as Bcl-xL, prevents Bax activation. This inhibition is relieved by BH3-only proteins, of which the effect can be mimicked by BH3-mimetics (Diepstraten et al., 2021, for review). We designed an experimental setup to test if Tom22 was required when Bax was primed by its engagement with Bcl-xL then release by WEHI-539. Bax and Bcl-xL were co-synthesized and co-inserted in nanodiscs formed with His7-tagged MSP1E3D1 (Rouchidane Eyitayo et al, 2023b). These nanodiscs were then purified and incubated in the presence of nanodiscs formed with StrepII-tagged MSP1E3D1, either empty or containing Tom22. The addition of WEHI-539 is expected to break the interaction between Bax and Bcl-xL, and to release Bax under a primed conformation (Gautier et al, 2011). StrepII-tagged nanodiscs were then purified and the presence of Bax was measured (Fig.5F). We observed that Bax was translocated to StrepII-nanodiscs containing Tom22, but not to empty StrepII-nanodiscs. This showed that the presence of Tom22 was required for Bax insertion after it was primed through its engagement with Bcl-xL followed by its release by WEHI-539.

Discussion

Tom22-induced conformational changes led to Bax membrane-insertion

Setting up a model combining the cell-free synthesis of Bax to its insertion into nanodiscs led us to reassess the involvement of the mitochondrial receptor Tom22 in Bax membrane insertion. We had previously reported that the presence of nanodiscs unexpectedly induced the precipitation of Bax (Rouchidane Eyitayo et al., 2023a). In the present study, we report that the co-synthesis of Tom22 prevented this precipitation (Fig.1AB). To decipher the mechanisms underlying the effect of Tom22, we investigated the molecular events leading to nanodisc-induced Bax precipitation.

We showed that the interaction of Bax with nanodiscs induced the exposure of the GALLL motif in Hα1 of Bax molecules resulting in their precipitation through hydrophobic interactions: indeed,

substitutions to more hydrophilic residues ($A^{24}R$, $L^{26}Q$) prevented Bax precipitation (Fig.2G). Conversely, the deletion of ART, that constitutively exposes Hα1 (Cartron et al., 2003), induced the precipitation of Bax, even in the absence of nanodiscs (Fig.2B).

The same GALLL motif is involved in the MOM targeting of Bax (Cartron et al., 2003) and in the interaction between Bax and Tom22 (Bellot et al., 2007). Knocking down Tom22, or inactivating it by proteolysis or by a specific antibody, decreased Bax mitochondrial localization, and apoptosis (Bellot et al., 2007). In the same study, peptide-mapping identified ^{22}KTGALLLQ^{28} as the main domain of interaction of Bax with Tom22. However, the involvement of Tom22 in Bax mitochondrial targeting has been debated, and contradictory conclusions have been drawn (Bellot et al., 2007; Ott et al., 2007; Sanjuán-Sklarz et al., 2007; Cartron et al., 2008; Colin et al., 2009; Ross et al., 2009). The present report, based on a minimal model containing only Bax, Tom22 and a lipid bilayer in nanodiscs, unambiguously demonstrated that Tom22 not only prevented Bax precipitation but further promoted its insertion into nanodiscs (Fig.1C-E). As summarized in Fig.6A, once the GALLL motif is exposed, it can be recognized by Tom22 which triggers Bax membrane insertion. In the absence of Tom22, the hydrophobic interaction between GALLL motifs led to Bax precipitation. Fig.6B illustrates the consequence of mutations in the GALLL motif, which prevented Bax precipitation but impaired the recognition by Tom22, while the deletion of ART constitutively exposed the GALLL motif leading to Bax precipitation in the absence of nanodiscs.

The membrane insertion of Bax requires the extrusion of Hα9 from the hydrophobic groove (Wolter et al., 1997; Suzuki et al., 2000; Czabotar et al, 2009, for review). Because of the stability of the interaction between residues S^{184} in Hα9 and D^{98} in Hα4, it is unlikely that Hα9 can be displaced by a BH3 domain, unless a previous conformational change destabilizing this interaction took place (Suzuki et al., 2000). It has been proposed that the interaction of Bim at the non-canonical binding site, including Hα1, Hα6 and the α1-α2 loop (Gavathiotis et al., 2008) could trigger long range conformational changes leading to Hα9 extrusion (Gavathiotis et al., 2010), which was further supported by molecular simulations (Jiang et al., 2016). Conformational changes induced by mutations in the α1-α2 loop actually induced the extrusion of Hα9 (Dengler et al., 2021). We report that the interaction of Tom22 with exposed Hα1 led to the insertion of Hα9 (Fig.3B). Conversely, the deletion of Hα9 or the introduction of the helix-breaking mutation $T^{174}P$ abolished the protective effect of Tom22 on Bax precipitation (Fig.3CE). This showed that, after Hα1 has been exposed, any failure of Hα9 membrane-insertion resulted in Bax precipitation, further emphasizing the crucial role of Hα9-

extrusion as the key step towards Bax insertion.

We next showed that Tom22-triggered conformational changes involved the residue D^{154} in Hα7: indeed, a substitution $D^{154}Y$, that is present in some tumors, did not prevent the rescue of Bax precipitation by Tom22 (Fig.4A), but impaired Bax insertion (Fig.4B) (Fig.6B). This suggests that the Tom22-triggered conformational change may involve D^{154}. Docking simulations between Bax and Tom22 suggested that Tom22 might interact more strongly with soluble Bax than with Hα9-inserted Bax (Veresov and Davidovskii, 2014). In the same study, simulating the breaking of the hydrogen bond between S^{184} and D^{98} resulted in the movement of the C-terminus of Bax, starting at D^{154}. These data are consistent with a transient interaction between Tom22 and soluble Bax, followed by a movement of the C-terminus of Bax around D^{154}, leading to Hα9 insertion and then the release of membrane-inserted Bax from the interaction with Tom22.

Furthermore, the possible occurrence of an electrostatic interaction of D^{154} with R^9 of ART stabilizing soluble Bax (Arokium et al., 2007) led us to study the consequences of the R^9E substitution. This mutant did not precipitate in the presence of nanodiscs (Fig.4C) and was spontaneously inserted (Fig.4DE) in a way that depended on Hα9 (Fig.4FG). This mutation thus fully recapitulated the effect of Tom22 (Fig.6B). Interestingly, $BaxR^9$ can be monomethylated (Larsen et al., 2016), which, similar to the R^9E substitution, is expected to destabilize the interaction with D^{154} and might therefore induce its spontaneous insertion, independently from Tom22.

Tom22-dependent Bax pore formation

Both BaxWT co-synthesized with Tom22 and $BaxR^9E$ synthesized alone were able to permeabilize liposomes to dextran-10kDa (Fig.5AB) and to form nanodiscs containing a pore displaying a ~5nm diameter (Fig.5C-E), which is consistent with electrophysiology data on MOM (Pavlov et al., 2001; Dejean et al., 2005; Guihard et al., 2004) and reconstituted Bax oligomers (Dejean et al., 2005). This size is much smaller than large structures observed by high resolution fluorescence microscopy and atomic force microscopy, reaching 24 to 176 nm in diameter (Salvador-Gallego et al., 2016; Große et al., 2016), which are compatible with the formation of megapores possibly involved in the release of mtDNA during inflammatory responses (McArthur et al., 2018; Cosentino et al., 2022). Conversely, the smaller 5nm-pore might correspond to the early apoptotic steps, when small apoptogenic factors, such as cytochrome c (~3nm) and smac/diablo (~3.5nm) are released. It is however larger than the 3.5nm size that had been measured with Bid-BH3/low pH-activated Bax co-formed in nanodiscs (Xu et

al., 2013). On the basis on cryoEM images and molecular dynamics, it was proposed that Bax monomers (or possibly dimers) could form lipidic pores by rearranging phospholipid molecules in nanodiscs (López et al., 2019). NMR studies of the Bax core (BaxHα2-Hα5) in bicelles are compatible with a pore of which walls included Bax dimers interacting with lipids, which might be further assembled to generate a pore large enough to promote the release of hydrated cytochrome c (Lv et al., 2021). Electrophysiology data showed that Bax pores exist under the form of oligomers containing a variable number of units, displaying different conductances (Martinez-Caballero et al., 2009), which might accurately describe the continuum of Bax-induced permeabilization to small apoptogenic factors including cytochrome c and smac/diablo, then to larger apoptogenic factors AIF and endonuclease G, and up to massive permeability events leading to the release of mitochondrial DNA in inflammatory responses (Wolf et al., 2022; Andrews, 2022; Vandenabeele et al., 2023; for reviews). However, there is no reason to assume that the conformation of membrane Bax in "small apoptotic pores" and "large inflammation pores" is identical. Although they exhibit a certain degree of flexibility (Shih et al., 2005), the nature of nanodiscs imposes more physical constraints on lipid packing than, for example, liposomes (Real-Hernandez and Levental, 2023). Bim and cBid are sufficient to insert Bax into liposomes (Shamas-Din et al., 2015), but not into nanodiscs (Fig.S3). It is tempting to speculate that this might reflect distinct conformations of Bax and, subsequently, different types of pores.

On the respective roles of BH3 direct activators and Tom22 on Bax membrane insertion and pore formation.

It has been shown that the induction of apoptosis was a prerequisite for Bax/Tom22 interaction *in cellulo* (Bellot et al., 2007). It can then be hypothesized that BH3 activators and Tom22 might cooperate during the process of Bax activation. The concerted action of Bim and Tom22 would lead to the extrusion then membrane insertion of Bax (Fig.6C). Once inserted, it has been shown that Bax could actually play the role of a receptor to itself (Tan et al., 2006). The interaction of Bax with cBid, that induces the exposure of the BH3-domain and the conformational change of Hα5/Hα6 (Czabotar et al., 2013), might therefore prime soluble Bax for its interaction with membrane-inserted Bax, leading to the step-wise formation of oligomers (Fig.6C).

In our minimal model, BH3 activators were not required, and the interaction of Bax with the lipid bilayer was sufficient to expose Hα1. The difference with *in cellulo* experiments is the presence of anti-apoptotic proteins, such as Bcl-xL. We then explored the involvement of Tom22 when Bax is inhibited

by Bcl-xL, then released by the BH3-mimetic WEHI-539. We first observed that Bax could be translocated and inserted into new nanodiscs only if Tom22 was present (Fig.5F, S5). This demonstrated that Tom22 was required for Bax membrane insertion after it was primed by the engagement then release of its interaction with Bcl-xL (Gautier et al., 2011). This emphasized the crucial role of Tom22 in Bax MOM-insertion under conditions where Bax was interacting with its anti-apoptotic partner, then released and primed by the rupture of this interaction. This might be fully relevant in the context of the use of BH3-mimetics as anti-tumor agents.

Conclusion

This study highlights the crucial role of Tom22 in Bax membrane insertion through its Hα9, that has been overlooked, since the first report showing that this receptor was involved in the MOM-targeting of Bax (Bellot et al., 2007). It also explains why Bax could not be spontaneously inserted in nanodiscs (Rouchidane Eyitayo et al., 2023a). This is paving the path for future structural studies on Bax in nanodiscs, in which Bax forms a relatively small pore, consistent with the limited release of small proteins such as cytochrome c. We also propose a model combining the action of Tom22 and BH3-activators Bim and cBid on Bax insertion, and extend our observations to the role of Tom22 in the membrane-insertion of Bax after it is released from its inhibition by Bcl-xL.

Materials and methods

Plasmids construction and cell-free protein synthesis

Bax, Tom22, Tom20 and Bcl-xL were cloned in the Nde1/Xho1 sites of the pIVEX 2.3a plasmid. Kras4b was cloned in the pIVEX 2.4 plasmid in frame with the N-terminal His6 tag. A double TAA stop codon was included to secure translation arrest during *in vitro* synthesis. Site-directed mutagenesis was done by an optimized Quickchange protocol (Liu and Naismith, 2008) and mutations were verified by sequencing (Eurofins).

The plasmid pET28b encoding His7-MSP1E3D1 (Addgene) was transformed into *E. coli* BL21DE3 and the protein was purified as described previously (Rouchidane Eyitayo et al., 2023ab). A strepII-tagged version of the protein has been constructed by site-directed mutagenesis. The pAR1219 encoding T7-RNA polymerase was transformed into E.coli BL21DE3*, and the protein was purified according to Larrieu et al. (2017). Nanodiscs have been formed with a mixture of phospholipids (48% POPC, 32% POPE, 12% DOPS, 8% cardiolipid (w/w)) (Anatrace). The cell-free synthesis protocol is

based on Larrieu et al. (2017) with some minor modifications (Rouchidane Eyitayo et al., 2023ab). Syntheses were done in inverted microtubes containing 100µL of Reaction Mix in the round compartment of the cap and 1700µL of Feeding Mix, separated by a dialysis membrane (cut-off 8-10kDa) overnight at 28°C under gentle agitation (80 rpm).

After the syntheses, the volume of the reaction mixes was carefully measured and, after a 20,000 x g centrifugation, the pellet was re-suspended in the same volume, so that the same proportions of pellets and supernatants were loaded on SDS-PAGE. After the separation of nanodiscs and soluble proteins on Ni-NTA (Qiagen), the same proportions of unbound material and imidazole-eluted material were analyzed (Fig.S6). It follows that, for each gel, the amount of proteins in pellets (p) *v/s* supernatants (sn), and in unbound fraction (u) *v/s* bound fraction (b) are directly comparable (see Rouchidane Eyitayo et al., 2023ab, for detailed protocols).

SDS-PAGE and Western blots

Proteins were solubilized in Laemmli buffer 2X and heated at 65°C for 20 minutes. Samples were loaded on SDS-PAGE (Mini Protean, Biorad). Tris-glycine gels were made of 12.5% of acrylamide/bisacrylamide (40/1). Gels were run at 15mA per gel. Protein transfer on PVDF membranes (Hybond, Cytiva) was done with the Transblot system (Biorad) for 1h30 at 350mA. Western-blotting was done in PBS or TBS, depending on the antibody (see Supplementary Table S7). Western-Blots were revealed by chimioluminescence (Luminata Forte, Millipore) and recorded with a digital camera (G-Box, Syngene).

NEM-PEG labeling

NEM-PEG labeling was done according to Dengler et al. (2021). Protein samples were incubated with 0.2mM methoxypolyethyleneglycol maleimide (5kDa; Sigma-Aldrich) for 1 minute on ice. The reaction was stopped by adding 20mM NEM for 10 minutes.

Dextran-FITC release from liposomes

Liposomes permeabilization was measured through the quenching of external Dextran-FITC by an anti-FITC antibody. A cell-free synthesis reaction was set-up in 100µL, in the presence of 10µL liposomes loaded with Dextran-FITC (10kDa, Sigma) (liposomes preparation is detailed in Rouchidane Eyitayo et al., 2023a). 4µg of anti-FITC antibody (Rabbit Monoclonal 6HC5LC9; ThermoFisher Scientific) was

added to quench external FITC fluorescence. The mix was then added to black 96-well plates and incubated at 28°C in a fluorescence plate reader (Clariostar, BMG Labtech). Fluorescence was measured at 10-minutes intervals (ex: 475-490 nm, em: 515-545 nm).

Bax translocation between nanodiscs

Bax and Bcl-xL were co-synthesized in the presence of nanodiscs formed with His7-tagged MSP and purified on Ni-NTA and dialyzed in ND buffer (200mM NaCl, 10mM Hepes, pH 7.4) to eliminate imidazole (Rouchidane Eyitayo et al., 2023b). In parallel experiments Tom22 was synthesized in the presence of nanodiscs formed with StrepII-tagged MSP, purified on Strep-Tactin (IBA) and dialyzed in ND buffer to eliminate biotin. The eluate from Ni-NTA containing Bax/Bcl-xL in His7-nanodiscs was mixed with an equal amount of StrepII-nanodiscs, empty or containing Tom22 (1.13 µM of each type of nanodiscs, expressed as MSP concentration). 250nM WEHI-539 was added to the mixes, that were incubated overnight at 4°C. Mixes were then loaded on Strep-Tactin and the unbound and bound fractions were collected and analyzed.

Dynamic Light Scattering

Dynamic Light Scattering (DLS) was measured in a DynaPro Nanostar (Wyatt) on 10µL samples. Triplicates of 10-acquisition measurements were done and averaged for each point.

Transmission Electron Microscopy

Transmission Electron Microscopy (TEM) was done as described previously (Rouchidane Eyitayo et al., 2023a). Nanodiscs were concentrated on Vivaspin concentrators (50kDa, Sartorius). Negative staining was done according to Daury et al. (2016). Samples were observed on a Tecnai F20 FEG electron microscope (FEI, ThermoFisher Scientific) operated at 200 kV using an Eagle 4k_4k camera (ThermoFisher Scientific). Measurements were manually done with Image J (https://imagej.net/ij/) on dm3 files.

Miscellaneous

Unless indicated otherwise, chemicals were from Clinisciences or Sigma-Aldrich.

Displayed blots are representative of at least 3 independent syntheses. When relevant, quantification has been done on non-saturated blots and statistical analyses were done with GraphPad 6.05 tools.

Acknowledgments

This work was supported by the CNRS, the University of Bordeaux and the Ligue Régionale contre le Cancer - Comité Gironde (n°267317 to S.M.). A.R.E. was recipient of a PhD fellowship from the Agence Nationale des Bourses du Gabon (ANBG).

References

Andrews DW. The case for brakes: Why restrain the size of Bax and Bak pores in outer mitochondrial membranes? Mol Cell. 2022 Mar 3;82(5):882-883. doi: 10.1016/j.molcel.2022.02.022. PMID: 35245452.

Antonsson B, Montessuit S, Lauper S, Eskes R, Martinou JC. Bax oligomerization is required for channel-forming activity in liposomes and to trigger cytochrome c release from mitochondria. Biochem J. 2000 Jan 15;345 Pt 2(Pt 2):271-8. PMID: 10620504; PMCID: PMC1220756.

Arokium H, Camougrand N, Vallette FM, Manon S. Studies of the interaction of substituted mutants of BAX with yeast mitochondria reveal that the C-terminal hydrophobic alpha-helix is a second ART sequence and plays a role in the interaction with anti-apoptotic BCL-xL. J Biol Chem. 2004 Dec 10;279(50):52566-73. doi: 10.1074/jbc.M408373200. Epub 2004 Sep 30. PMID: 15459197.

Arokium H, Ouerfelli H, Velours G, Camougrand N, Vallette FM, Manon S. Substitutions of potentially phosphorylatable serine residues of Bax reveal how they may regulate its interaction with mitochondria. J Biol Chem. 2007 Nov 30;282(48):35104-12. doi: 10.1074/jbc.M704891200. Epub 2007 Oct 2. PMID: 17911107.

Barclay LA, Wales TE, Garner TP, Wachter F, Lee S, Guerra RM, Stewart ML, Braun CR, Bird GH, Gavathiotis E, Engen JR, Walensky LD. Inhibition of Pro-apoptotic BAX by a noncanonical interaction mechanism. Mol Cell. 2015 Mar 5;57(5):873-886. doi: 10.1016/j.molcel.2015.01.014. Epub 2015 Feb 12. PMID: 25684204; PMCID: PMC4384643.

Bellot G, Cartron PF, Er E, Oliver L, Juin P, Armstrong LC, Bornstein P, Mihara K, Manon S, Vallette FM. TOM22, a core component of the mitochondria outer membrane protein translocation pore, is a mitochondrial receptor for the proapoptotic protein Bax. Cell Death Differ. 2007 Apr;14(4):785-94. doi: 10.1038/sj.cdd.4402055. Epub 2006 Nov 10. PMID: 17096026.

Bleicken S, Assafa TE, Stegmueller C, Wittig A, Garcia-Saez AJ, Bordignon E. Topology of active, membrane-embedded Bax in the context of a toroidal pore. Cell Death Differ. 2018 Nov;25(10):1717-1731. doi: 10.1038/s41418-018-0184-6. Epub 2018 Sep 5. PMID: 30185826; PMCID: PMC6180131.

Cartron PF, Oliver L, Martin S, Moreau C, LeCabellec MT, Jezequel P, Meflah K, Vallette FM. The expression of a new variant of the pro-apoptotic molecule Bax, Baxpsi, is correlated with an increased survival of glioblastoma multiforme patients. Hum Mol Genet. 2002 Mar 15;11(6):675-87. doi: 10.1093/hmg/11.6.675. PMID: 11912183.

Cartron PF, Priault M, Oliver L, Meflah K, Manon S, Vallette FM. The N-terminal end of Bax contains a mitochondrial-targeting signal. J Biol Chem. 2003 Mar 28;278(13):11633-41. doi: 10.1074/jbc.M208955200. Epub 2003 Jan 15. PMID: 12529375.

Cartron PF, Arokium H, Oliver L, Meflah K, Manon S, Vallette FM. Distinct domains control the addressing and the insertion of Bax into mitochondria. J Biol Chem. 2005 Mar 18;280(11):10587-98. doi: 10.1074/jbc.M409714200. Epub 2004 Dec 7. PMID: 15590655.

Cartron PF, Bellot G, Oliver L, Grandier-Vazeille X, Manon S, Vallette FM. Bax inserts into the mitochondrial outer membrane by different mechanisms. FEBS Lett. 2008 Sep 3;582(20):3045-51. doi: 10.1016/j.febslet.2008.07.047. Epub 2008 Aug 5. PMID: 18687331.

Cartron PF, Petit E, Bellot G, Oliver L, Vallette FM. Metaxins 1 and 2, two proteins of the mitochondrial protein sorting and assembly machinery, are essential for Bak activation during TNF alpha triggered apoptosis. Cell Signal. 2014 Sep;26(9):1928-34. doi: 10.1016/j.cellsig.2014.04.021. Epub 2014 May 2. PMID: 24794530.

Cheng EH, Sheiko TV, Fisher JK, Craigen WJ, Korsmeyer SJ. VDAC2 inhibits BAK activation and mitochondrial apoptosis. Science. 2003 Jul 25;301(5632):513-7. doi: 10.1126/science.1083995. PMID: 12881569.

Colin J, Garibal J, Mignotte B, Guénal I. The mitochondrial TOM complex modulates bax-induced apoptosis in Drosophila. Biochem Biophys Res Commun. 2009 Feb 20;379(4):939-43. doi: 10.1016/j.bbrc.2008.12.176. Epub 2009 Jan 10. PMID: 19138672.

Cosentino K, Hertlein V, Jenner A, Dellmann T, Gojkovic M, Peña-Blanco A, Dadsena S, Wajngarten N, Danial JSH, Thevathasan JV, Mund M, Ries J, Garcia-Saez AJ. The interplay between BAX and BAK tunes apoptotic pore growth to control mitochondrial-DNA-mediated inflammation. Mol Cell. 2022 Mar 3;82(5):933-949.e9. doi: 10.1016/j.molcel.2022.01.008. Epub 2022 Feb 3. PMID: 35120587; PMCID: PMC8901441.

Czabotar PE, Colman PM, Huang DC. Bax activation by Bim? Cell Death Differ. 2009 Sep;16(9):1187-91. doi: 10.1038/cdd.2009.83. Epub 2009 Jun 26. PMID: 19557009.

Czabotar PE, Westphal D, Dewson G, Ma S, Hockings C, Fairlie WD, Lee EF, Yao S, Robin AY, Smith BJ, Huang DC, Kluck RM, Adams JM, Colman PM. Bax crystal structures reveal how BH3 domains activate Bax and nucleate its oligomerization to induce apoptosis. Cell. 2013 Jan 31;152(3):519-31. doi: 10.1016/j.cell.2012.12.031. PMID: 23374347.

Czabotar PE, Garcia-Saez AJ. Mechanisms of BCL-2 family proteins in mitochondrial apoptosis. Nat Rev Mol Cell Biol. 2023 Oct;24(10):732-748. doi: 10.1038/s41580-023-00629-4. Epub 2023 Jul 12. PMID: 37438560.

Daury L, Orange F, Taveau JC, Verchère A, Monlezun L, Gounou C, Marreddy RK, Picard M, Broutin I, Pos KM, Lambert O. Tripartite assembly of RND multidrug efflux pumps. Nat Commun. 2016 Feb 12;7:10731. doi: 10.1038/ncomms10731. PMID: 26867482; PMCID: PMC4754349.

Dejean LM, Martinez-Caballero S, Guo L, Hughes C, Teijido O, Ducret T, Ichas F, Korsmeyer SJ,

Antonsson B, Jonas EA, Kinnally KW. Oligomeric Bax is a component of the putative cytochrome c release channel MAC, mitochondrial apoptosis-induced channel. Mol Biol Cell. 2005 May;16(5):2424-32. doi: 10.1091/mbc.e04-12-1111. Epub 2005 Mar 16. PMID: 15772159; PMCID: PMC1087246.

Dengler MA, Gibson L, Adams JM. BAX mitochondrial integration is regulated allosterically by its α1-α2 loop. Cell Death Differ. 2021 Dec;28(12):3270-3281. doi: 10.1038/s41418-021-00815-x. Epub 2021 Jun 16. PMID: 34135480; PMCID: PMC8630029.

Desagher S, Osen-Sand A, Nichols A, Eskes R, Montessuit S, Lauper S, Maundrell K, Antonsson B, Martinou JC. Bid-induced conformational change of Bax is responsible for mitochondrial cytochrome c release during apoptosis. J Cell Biol. 1999 Mar 8;144(5):891-901. doi: 10.1083/jcb.144.5.891. PMID: 10085289; PMCID: PMC2148190.

Diepstraten ST, Anderson MA, Czabotar PE, Lessene G, Strasser A, Kelly GL. The manipulation of apoptosis for cancer therapy using BH3-mimetic drugs. Nat Rev Cancer. 2022 Jan;22(1):45-64. doi: 10.1038/s41568-021-00407-4. Epub 2021 Oct 18. PMID: 34663943.

García-Nafría J, Tate CG. Structure determination of GPCRs: cryo-EM compared with X-ray crystallography. Biochem Soc Trans. 2021 Nov 1;49(5):2345-2355. doi: 10.1042/BST20210431. PMID: 34581758; PMCID: PMC8589417.

Gautier F, Guillemin Y, Cartron PF, Gallenne T, Cauquil N, Le Diguarher T, Casara P, Vallette FM, Manon S, Hickman JA, Geneste O, Juin P. Bax activation by engagement with, then release from, the BH3 binding site of Bcl-xL. Mol Cell Biol. 2011 Feb;31(4):832-44. doi: 10.1128/MCB.00161-10. Epub 2010 Dec 20. PMID: 21173168; PMCID: PMC3028639.

Gavathiotis E, Suzuki M, Davis ML, Pitter K, Bird GH, Katz SG, Tu HC, Kim H, Cheng EH, Tjandra N, Walensky LD. BAX activation is initiated at a novel interaction site. Nature. 2008 Oct 23;455(7216):1076-81. doi: 10.1038/nature07396. PMID: 18948948; PMCID: PMC2597110.

Gavathiotis E, Reyna DE, Davis ML, Bird GH, Walensky LD. BH3-triggered structural reorganization

drives the activation of proapoptotic BAX. Mol Cell. 2010 Nov 12;40(3):481-92. doi: 10.1016/j.molcel.2010.10.019. PMID: 21070973; PMCID: PMC3050027.

Goping IS, Gross A, Lavoie JN, Nguyen M, Jemmerson R, Roth K, Korsmeyer SJ, Shore GC. Regulated targeting of BAX to mitochondria. J Cell Biol. 1998 Oct 5;143(1):207-15. doi: 10.1083/jcb.143.1.207. PMID: 9763432; PMCID: PMC2132805.

Green DR. The Mitochondrial Pathway of Apoptosis Part II: The BCL-2 Protein Family. Cold Spring Harb Perspect Biol. 2022 Jun 14;14(6):a041046. doi: 10.1101/cshperspect.a041046. PMID: 35701220; PMCID: PMC9248827.

Große L, Wurm CA, Brüser C, Neumann D, Jans DC, Jakobs S. Bax assembles into large ring-like structures remodeling the mitochondrial outer membrane in apoptosis. EMBO J. 2016 Feb 15;35(4):402-13. doi: 10.15252/embj.201592789. Epub 2016 Jan 18. PMID: 26783364; PMCID: PMC4755111.

Guihard G, Bellot G, Moreau C, Pradal G, Ferry N, Thomy R, Fichet P, Meflah K, Vallette FM. The mitochondrial apoptosis-induced channel (MAC) corresponds to a late apoptotic event. J Biol Chem. 2004 Nov 5;279(45):46542-50. doi: 10.1074/jbc.M405153200. Epub 2004 Aug 24. PMID: 15328340.

Hsu YT, Youle RJ. Nonionic detergents induce dimerization among members of the Bcl-2 family. J Biol Chem. 1997 May 23;272(21):13829-34. doi: 10.1074/jbc.272.21.13829. PMID: 9153240.

Jenner A, Peña-Blanco A, Salvador-Gallego R, Ugarte-Uribe B, Zollo C, Ganief T, Bierlmeier J, Mund M, Lee JE, Ries J, Schwarzer D, Macek B, Garcia-Saez AJ. DRP1 interacts directly with BAX to induce its activation and apoptosis. EMBO J. 2022 Apr 19;41(8):e108587. doi: 10.15252/embj.2021108587. Epub 2022 Jan 13. PMID: 35023587; PMCID: PMC9016351.

Jiang Z, Zhang H, Böckmann RA. Allostery in BAX protein activation. J Biomol Struct Dyn. 2016 Nov;34(11):2469-80. doi: 10.1080/07391102.2015.1119731. Epub 2016 Feb 6. PMID: 26578184.

Kale J, Kutuk O, Brito GC, Andrews TS, Leber B, Letai A, Andrews DW. Phosphorylation switches Bax from promoting to inhibiting apoptosis thereby increasing drug resistance. EMBO Rep. 2018 Sep;19(9):e45235. doi: 10.15252/embr.201745235. Epub 2018 Jul 9. PMID: 29987135; PMCID: PMC6123645.

Kaufmann T, Schlipf S, Sanz J, Neubert K, Stein R, Borner C. Characterization of the signal that directs Bcl-x(L), but not Bcl-2, to the mitochondrial outer membrane. J Cell Biol. 2003 Jan 6;160(1):53-64. doi: 10.1083/jcb.200210084. Epub 2003 Jan 6. PMID: 12515824; PMCID: PMC2172731.

Lalier L, Mignard V, Joalland MP, Lanoé D, Cartron PF, Manon S, Vallette FM. TOM20-mediated transfer of Bcl2 from ER to MAM and mitochondria upon induction of apoptosis. Cell Death Dis. 2021 Feb 15;12(2):182. doi: 10.1038/s41419-021-03471-8. PMID: 33589622; PMCID: PMC7884705.

Lalier L, Vallette F, Manon S. Bcl-2 Family Members and the Mitochondrial Import Machineries: The Roads to Death. Biomolecules. 2022 Jan 19;12(2):162. doi: 10.3390/biom12020162. PMID: 35204663; PMCID: PMC8961529.

Larsen SC, Sylvestersen KB, Mund A, Lyon D, Mullari M, Madsen MV, Daniel JA, Jensen LJ, Nielsen ML. Proteome-wide analysis of arginine monomethylation reveals widespread occurrence in human cells. Sci Signal. 2016 Aug 30;9(443):rs9. doi: 10.1126/scisignal.aaf7329. PMID: 27577262.

Lauterwasser J, Todt F, Zerbes RM, Nguyen TN, Craigen W, Lazarou M, van der Laan M, Edlich F. The porin VDAC2 is the mitochondrial platform for Bax retrotranslocation. Sci Rep. 2016 Sep 13;6:32994. doi: 10.1038/srep32994. PMID: 27620692; PMCID: PMC5020405.

Lee KY, Ikura M, Marshall CB. The Self-Association of the KRAS4b Protein is Altered by Lipid-Bilayer Composition and Electrostatics. Angew Chem Int Ed Engl. 2023 Apr 24;62(18):e202218698. doi: 10.1002/anie.202218698. Epub 2023 Mar 27. PMID: 36883374.

Liu H, Naismith JH. An efficient one-step site-directed deletion, insertion, single and multiple-site

plasmid mutagenesis protocol. BMC Biotechnol. 2008 Dec 4;8:91. doi: 10.1186/1472-6750-8-91. PMID: 19055817; PMCID: PMC2629768.

López CA, Swift MF, Xu XP, Hanein D, Volkmann N, Gnanakaran S. Biophysical Characterization of a Nanodisc with and without BAX: An Integrative Study Using Molecular Dynamics Simulations and Cryo-EM. Structure. 2019 Jun 4;27(6):988-999.e4. doi: 10.1016/j.str.2019.03.013. Epub 2019 Apr 11. PMID: 30982634.

Lv F, Qi F, Zhang Z, Wen M, Kale J, Piai A, Du L, Wang S, Zhou L, Yang Y, Wu B, Liu Z, Del Rosario J, Pogmore J, Chou JJ, Andrews DW, Lin J, OuYang B. An amphipathic Bax core dimer forms part of the apoptotic pore wall in the mitochondrial membrane. EMBO J. 2021 Jul 15;40(14):e106438. doi: 10.15252/embj.2020106438. Epub 2021 Jun 8. PMID: 34101209; PMCID: PMC8280806.

Ma SB, Nguyen TN, Tan I, Ninnis R, Iyer S, Stroud DA, Menard M, Kluck RM, Ryan MT, Dewson G. Bax targets mitochondria by distinct mechanisms before or during apoptotic cell death: a requirement for VDAC2 or Bak for efficient Bax apoptotic function. Cell Death Differ. 2014 Dec;21(12):1925-35. doi: 10.1038/cdd.2014.119. Epub 2014 Aug 22. PMID: 25146925; PMCID: PMC4227151.

Marani M, Tenev T, Hancock D, Downward J, Lemoine NR. Identification of novel isoforms of the BH3 domain protein Bim which directly activate Bax to trigger apoptosis. Mol Cell Biol. 2002 Jun;22(11):3577-89. doi: 10.1128/MCB.22.11.3577-3589.2002. PMID: 11997495; PMCID: PMC133811.

Martin D, Abba MC, Molinolo AA, Vitale-Cross L, Wang Z, Zaida M, Delic NC, Samuels Y, Lyons JG, Gutkind JS. The head and neck cancer cell oncogenome: a platform for the development of precision molecular therapies. Oncotarget. 2014 Oct 15;5(19):8906-23. doi: 10.18632/oncotarget.2417. PMID: 25275298; PMCID: PMC4253406.

Martinez-Caballero S, Dejean LM, Kinnally MS, Oh KJ, Mannella CA, Kinnally KW. Assembly of the mitochondrial apoptosis-induced channel, MAC. J Biol Chem. 2009 May 1;284(18):12235-45. doi: 10.1074/jbc.M806610200. Epub 2009 Mar 4. PMID: 19261612; PMCID: PMC2673292.

McArthur K, Whitehead LW, Heddleston JM, Li L, Padman BS, Oorschot V, Geoghegan ND, Chappaz S, Davidson S, San Chin H, Lane RM, Dramicanin M, Saunders TL, Sugiana C, Lessene R, Osellame LD, Chew TL, Dewson G, Lazarou M, Ramm G, Lessene G, Ryan MT, Rogers KL, van Delft MF, Kile BT. BAK/BAX macropores facilitate mitochondrial herniation and mtDNA efflux during apoptosis. Science. 2018 Feb 23;359(6378):eaao6047. doi: 10.1126/science.aao6047. PMID: 29472455.

Motz C, Martin H, Krimmer T, Rassow J. Bcl-2 and porin follow different pathways of TOM-dependent insertion into the mitochondrial outer membrane. J Mol Biol. 2002 Nov 1;323(4):729-38. doi: 10.1016/s0022-2836(02)00995-6. PMID: 12419260.

Nargang FE, Rapaport D, Ritzel RG, Neupert W, Lill R. Role of the negative charges in the cytosolic domain of TOM22 in the import of precursor proteins into mitochondria. Mol Cell Biol. 1998 Jun;18(6):3173-81. doi: 10.1128/MCB.18.6.3173. PMID: 9584158; PMCID: PMC108899.

Notti RQ, Walz T. Native-like environments afford novel mechanistic insights into membrane proteins. Trends Biochem Sci. 2022 Jul;47(7):561-569. doi: 10.1016/j.tibs.2022.02.008. Epub 2022 Mar 21. PMID: 35331611; PMCID: PMC9847468.

Ott M, Norberg E, Walter KM, Schreiner P, Kemper C, Rapaport D, Zhivotovsky B, Orrenius S. The mitochondrial TOM complex is required for tBid/Bax-induced cytochrome c release. J Biol Chem. 2007 Sep 21;282(38):27633-9. doi: 10.1074/jbc.M703155200. Epub 2007 Jul 16. PMID: 17635912.

Ott M, Norberg E, Zhivotovsky B, Orrenius S. Mitochondrial targeting of tBid/Bax: a role for the TOM complex? Cell Death Differ. 2009 Aug;16(8):1075-82. doi: 10.1038/cdd.2009.61. Epub 2009 Jun 12. PMID: 19521421.

Pavlov EV, Priault M, Pietkiewicz D, Cheng EH, Antonsson B, Manon S, Korsmeyer SJ, Mannella CA, Kinnally KW. A novel, high conductance channel of mitochondria linked to apoptosis in mammalian cells and Bax expression in yeast. J Cell Biol. 2001 Nov 26;155(5):725-31. doi:

10.1083/jcb.200107057. Epub 2001 Nov 26. PMID: 11724814; PMCID: PMC2150879.

Petit E, Cartron PF, Oliver L, Vallette FM. The phosphorylation of Metaxin 1 controls Bak activation during TNFα induced cell death. Cell Signal. 2017 Jan;30:171-178. doi: 10.1016/j.cellsig.2016.11.008. Epub 2016 Nov 12. PMID: 27845183.

Peyerl FW, Dai S, Murphy GA, Crawford F, White J, Marrack P, Kappler JW. Elucidation of some Bax conformational changes through crystallization of an antibody-peptide complex. Cell Death Differ. 2007 Mar;14(3):447-52. doi: 10.1038/sj.cdd.4402025. Epub 2006 Sep 1. PMID: 16946732.

Real Hernandez LM, Levental I. Lipid packing is disrupted in copolymeric nanodiscs compared with intact membranes. Biophys J. 2023 Jun 6;122(11):2256-2266. doi: 10.1016/j.bpj.2023.01.013. Epub 2023 Jan 14. PMID: 36641625; PMCID: PMC10257115.

Reyna DE, Garner TP, Lopez A, Kopp F, Choudhary GS, Sridharan A, Narayanagari SR, Mitchell K, Dong B, Bartholdy BA, Walensky LD, Verma A, Steidl U, Gavathiotis E. Direct Activation of BAX by BTSA1 Overcomes Apoptosis Resistance in Acute Myeloid Leukemia. Cancer Cell. 2017 Oct 9;32(4):490-505.e10. doi: 10.1016/j.ccell.2017.09.001. PMID: 29017059; PMCID: PMC5793879.

Ross K, Rudel T, Kozjak-Pavlovic V. TOM-independent complex formation of Bax and Bak in mammalian mitochondria during TNFalpha-induced apoptosis. Cell Death Differ. 2009 May;16(5):697-707. doi: 10.1038/cdd.2008.194. Epub 2009 Jan 23. PMID: 19165229.

Rouchidane Eyitayo A, Giraud MF, Daury L, Lambert O, Gonzalez C, Manon S. Cell-free synthesis and reconstitution of Bax in nanodiscs: Comparison between wild-type Bax and a constitutively active mutant. Biochim Biophys Acta Biomembr. 2023 Jan 1;1865(1):184075. doi: 10.1016/j.bbamem.2022.184075. Epub 2022 Oct 20. PMID: 36273540.

Rouchidane Eyitayo A, Boudier-Lemosquet A, Chaignepain S, Priault M, Manon S. Bcl-xL Is Spontaneously Inserted into Preassembled Nanodiscs and Stimulates Bax Insertion in a Cell-Free Protein Synthesis System. Biomolecules. 2023 May 23;13(6):876. doi: 10.3390/biom13060876. PMID:

37371456; PMCID: PMC10296133.

Salvador-Gallego R, Mund M, Cosentino K, Schneider J, Unsay J, Schraermeyer U, Engelhardt J, Ries J, García-Sáez AJ. Bax assembly into rings and arcs in apoptotic mitochondria is linked to membrane pores. EMBO J. 2016 Feb 15;35(4):389-401. doi: 10.15252/embj.201593384. Epub 2016 Jan 18. PMID: 26783362; PMCID: PMC4755116.

Sanjuán Szklarz LK, Kozjak-Pavlovic V, Vögtle FN, Chacinska A, Milenkovic D, Vogel S, Dürr M, Westermann B, Guiard B, Martinou JC, Borner C, Pfanner N, Meisinger C. Preprotein transport machineries of yeast mitochondrial outer membrane are not required for Bax-induced release of intermembrane space proteins. J Mol Biol. 2007 Apr 20;368(1):44-54. doi: 10.1016/j.jmb.2007.01.016. Epub 2007 Jan 12. PMID: 17335847.

Schlesinger PH, Gross A, Yin XM, Yamamoto K, Saito M, Waksman G, Korsmeyer SJ. Comparison of the ion channel characteristics of proapoptotic BAX and antiapoptotic BCL-2. Proc Natl Acad Sci U S A. 1997 Oct 14;94(21):11357-62. doi: 10.1073/pnas.94.21.11357. PMID: 9326614; PMCID: PMC23466.

Sedlak TW, Oltvai ZN, Yang E, Wang K, Boise LH, Thompson CB, Korsmeyer SJ. Multiple Bcl-2 family members demonstrate selective dimerizations with Bax. Proc Natl Acad Sci U S A. 1995 Aug 15;92(17):7834-8. doi: 10.1073/pnas.92.17.7834. PMID: 7644501; PMCID: PMC41240.

Shamas-Din A, Bindner S, Chi X, Leber B, Andrews DW, Fradin C. Distinct lipid effects on tBid and Bim activation of membrane permeabilization by pro-apoptotic Bax. Biochem J. 2015 May 1;467(3):495-505. doi: 10.1042/BJ20141291. PMID: 25714678.

Shih AY, Denisov IG, Phillips JC, Sligar SG, Schulten K. Molecular dynamics simulations of discoidal bilayers assembled from truncated human lipoproteins. Biophys J. 2005 Jan;88(1):548-56. doi: 10.1529/biophysj.104.046896. Epub 2004 Nov 8. PMID: 15533924; PMCID: PMC1305032.

Simonyan L, Légiot A, Lascu I, Durand G, Giraud MF, Gonzalez C, Manon S. The substitution of

Proline 168 favors Bax oligomerization and stimulates its interaction with LUVs and mitochondria. Biochim Biophys Acta Biomembr. 2017 Jun;1859(6):1144-1155. doi: 10.1016/j.bbamem.2017.03.010. Epub 2017 Mar 16. PMID: 28322731.

Simonyan L, Gonin M, Hanks J, Friedlein J, Dutrec K, Arokium H, Rouchidane Eyitayo A, Doudy TM, Chaignepain S, Manon S, Dejean L. Non-phosphorylatable mutants of Ser184 lead to incomplete activation of Bax. Front Oncol. 2023 Jan 19;12:1068994. doi: 10.3389/fonc.2022.1068994. PMID: 36741728; PMCID: PMC9892840.

Suzuki M, Youle RJ, Tjandra N. Structure of Bax: coregulation of dimer formation and intracellular localization. Cell. 2000 Nov 10;103(4):645-54. doi: 10.1016/s0092-8674(00)00167-7. PMID: 11106734.

Tan C, Dlugosz PJ, Peng J, Zhang Z, Lapolla SM, Plafker SM, Andrews DW, Lin J. Auto-activation of the apoptosis protein Bax increases mitochondrial membrane permeability and is inhibited by Bcl-2. J Biol Chem. 2006 May 26;281(21):14764-75. doi: 10.1074/jbc.M602374200. Epub 2006 Mar 29. PMID: 16571718; PMCID: PMC2826894.

Thonghin N, Kargas V, Clews J, Ford RC. Cryo-electron microscopy of membrane proteins. Methods. 2018 Sep 1;147:176-186. doi: 10.1016/j.ymeth.2018.04.018. Epub 2018 Apr 25. PMID: 29702228.

Tremblais K, Oliver L, Juin P, Le Cabellec TM, Meflah K, Vallette FM. The C-terminus of bax is not a membrane addressing/anchoring signal. Biochem Biophys Res Commun. 1999 Jul 14;260(3):582-91. doi: 10.1006/bbrc.1999.0904. PMID: 10403809.

Vandenabeele P, Bultynck G, Savvides SN. Pore-forming proteins as drivers of membrane permeabilization in cell death pathways. Nat Rev Mol Cell Biol. 2023 May;24(5):312-333. doi: 10.1038/s41580-022-00564-w. Epub 2022 Dec 21. PMID: 36543934.

Veresov VG, Davidovskii AI. Structural insights into proapoptotic signaling mediated by MTCH2, VDAC2, TOM40 and TOM22. Cell Signal. 2014 Feb;26(2):370-82. doi: 10.1016/j.cellsig.2013.11.016.

Epub 2013 Nov 19. PMID: 24269536.

Westphal D, Dewson G, Menard M, Frederick P, Iyer S, Bartolo R, Gibson L, Czabotar PE, Smith BJ, Adams JM, Kluck RM. Apoptotic pore formation is associated with in-plane insertion of Bak or Bax central helices into the mitochondrial outer membrane. Proc Natl Acad Sci U S A. 2014 Sep 30;111(39):E4076-85. doi: 10.1073/pnas.1415142111. Epub 2014 Sep 16. PMID: 25228770; PMCID: PMC4191798.

Wolf P, Schoeniger A, Edlich F. Pro-apoptotic complexes of BAX and BAK on the outer mitochondrial membrane. Biochim Biophys Acta Mol Cell Res. 2022 Oct;1869(10):119317. doi: 10.1016/j.bbamcr.2022.119317. Epub 2022 Jun 22. PMID: 35752202.

Wolter KG, Hsu YT, Smith CL, Nechushtan A, Xi XG, Youle RJ. Movement of Bax from the cytosol to mitochondria during apoptosis. J Cell Biol. 1997 Dec 1;139(5):1281-92. doi: 10.1083/jcb.139.5.1281. PMID: 9382873; PMCID: PMC2140220.

Xu XP, Zhai D, Kim E, Swift M, Reed JC, Volkmann N, Hanein D. Three-dimensional structure of Bax-mediated pores in membrane bilayers. Cell Death Dis. 2013 Jun 20;4(6):e683. doi: 10.1038/cddis.2013.210. PMID: 23788040; PMCID: PMC3702287.

Yethon JA, Epand RF, Leber B, Epand RM, Andrews DW. Interaction with a membrane surface triggers a reversible conformational change in Bax normally associated with induction of apoptosis. J Biol Chem. 2003 Dec 5;278(49):48935-41. doi: 10.1074/jbc.M306289200. Epub 2003 Sep 30. PMID: 14522999.

Yuan Z, Dewson G, Czabotar PE, Birkinshaw RW. VDAC2 and the BCL-2 family of proteins. Biochem Soc Trans. 2021 Dec 17;49(6):2787-2795. doi: 10.1042/BST20210753. PMID: 34913469; PMCID: PMC8786305.

Figures

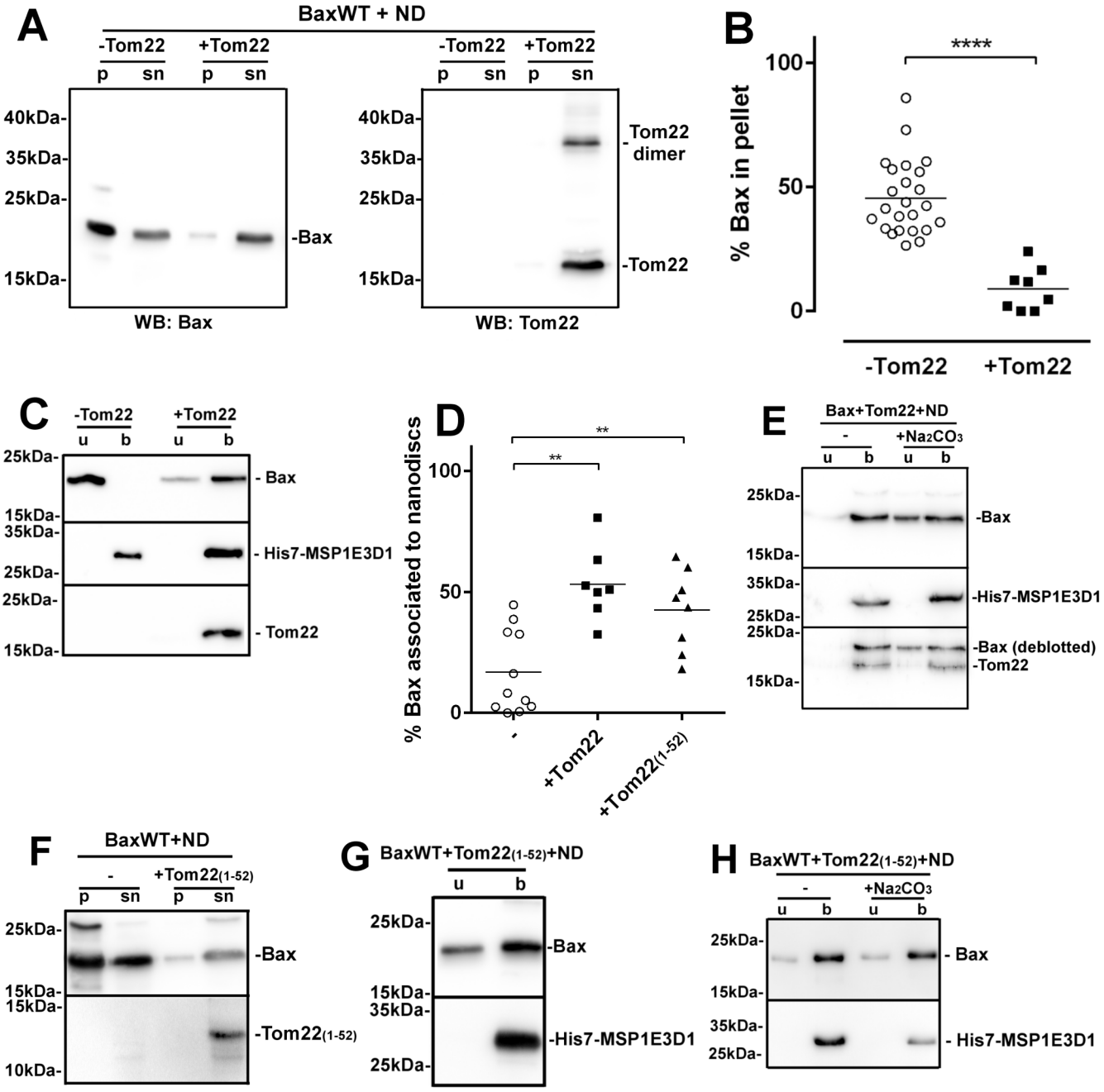

Figure 1: Tom22 co-synthesis prevents Bax-precipitation and promotes its insertion

(A) BaxWT was synthesized alone or co-synthesized with Tom22, in cell-free, in the presence of 3.5µM nanodiscs (ND). The amount ratio of piVEX plasmids encoding the two proteins was 2 to 1

(typically 15ng and 7.5ng for Bax and Tom22, respectively). After the synthesis, the reaction mix was weighed and centrifuged at 20,000 x g for 15 minutes. The pellet was resuspended in the same volume of buffer B (25mM Hepes/Na pH 7.4, 200mM NaCl, 0.1mM EDTA). Aliquots (typically 5µL) from both the pellet (p) and supernatant (sn) were mixed with an equal volume of Laemmli buffer 2X, and analyzed by SDS-PAGE and western-blot against Bax and Tom22. Note that Tom22 was visible under the forms of a monomer and a dimer. For the sake of clarity, only the monomer will be displayed in following experiments.

(B) Quantitative analyzis of the effect of the co-synthesis of Tom22 on nanodisc-induced Bax precipitation. Non-saturated western-blots similar to **(A)** were quantified with Image J and the % of Bax in the pellets was calculated. (****unpaired t-test, $p<0.0001$).

(C) The remaining supernatant (typically 85µL) was mixed with 100µL of Ni-NTA-agarose (Qiagen) pre-washed in buffer B, and incubated for 2 hours at 4°C under gentle agitation. The mixture was centrifuged (2000 x g, 30 seconds) and the unbound fraction (lanes u) was collected. The resin was then washed 3 times with 500µL buffer W (20mM Tris/HCl pH 8.0, 500mM NaCl). An identical volume as the unbound fraction of buffer E (20mM Tris/HCl pH8.0, 200mM NaCl, 300mM imidazole) was added to recover Ni^{2+}-bound nanodiscs) (lanes b). An identical volume of the unbound (u) and bound (b) fractions were mixed with an identical volume of Laemmli buffer 2X, and analyzed by SDS-PAGE and western-blot against Bax, Tom22 and His7-MSP1E3D1.

(D) Quantification of Bax bound to nanodiscs (b). Non-saturated western-blots similar to **(C)** were quantified with Image J and the % of Bax in fraction b was calculated. (**unpaired t-test, $p<0.01$).

(E) Purified nanodiscs in the fraction "b" of **(C)** were dialyzed against buffer D (20mM Tris/HCl pH 8.0, 200mM NaCl) to eliminate imidazole. They were then added with 100mM Na_2CO_3, pH 10.0 and incubated for 15 minutes. Nanodiscs were then re-purified on Ni-NTA, as in **(C)**.

(F,G,H) Same experiments as in **(A,C,E)** with $Tom22_{(1-52)}$ instead of full-length Tom22.

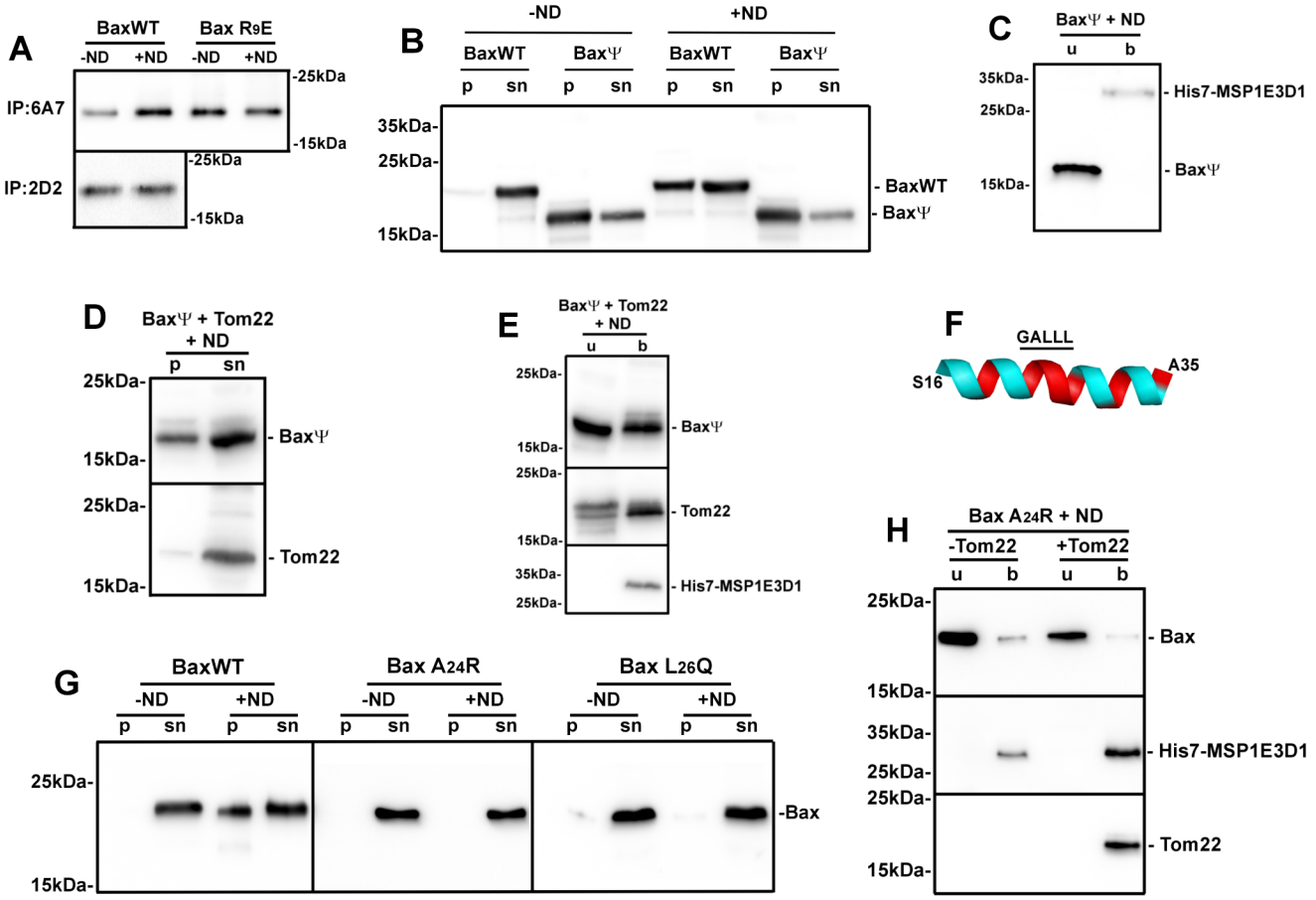

Figure 2. The GALLL motif in α1-helix is responsible for nanodisc-induced Bax precipitation, and interacts with Tom22.

(A) BaxWT and the constitutively active mutant BaxR9E were synthesized in the absence of nanodiscs. Reaction mixes were centrifuged (20,000 x g, 15 minutes) and equal volumes of the supernatants were added or not with 3.5µM nanodiscs. 1µg anti-Bax 6A7 or 2D2 antibodies (Santa-Cruz Biotechnology) were added and samples were incubated overnight at 4°C under gentle agitation. 50µL Protein-G sepharose beads (Cytiva) were washed with buffer IP (20mM Tris/HCl pH 8.0, 200mM NaCl) were added for 3 hours. The suspensions were then washed 5 times with 200µL of buffer WIP (25mM Tris/HCl pH 7.4, 500mM NaCl, 1mM EDTA, 1% Nonidet P-40, 10% glycerol) and twice with the same buffer diluted 10 times. Bound proteins were recovered by adding 30µL of Laemmli buffer (without β-mercaptoethanol) and heating at 65°C for 15 minutes. Samples were analyzed by SDS-PAGE and western-blot against Bax, with a distinct antibody from the ones used for immunoprecipitations (Abcam).

(B) BaxWT and BaxΨ (deleted of residues 1-19) were synthesized in the absence or the presence of nanodiscs and analyzed like in Fig.1A. Western-blots were done with the Abcam antibody of which the undisclosed epitope is away from the N-terminus.

(C) Supernatants from BaxΨ in **(B)** were analyzed as in Fig.1C, showing the absence of BaxΨ-association to nanodiscs.

(D) BaxΨ was co-synthesized with Tom22 in the presence of nanodiscs, and the sample were analyzed like in **(B)**.

(E) Supernatants from **(D)** were analyzed like in **(C)**, showing the partial association of BaxΨ to nanodiscs.

(F) Representation of the α1-helix of Bax in the 1F16 structure (Suzuki et al., 2000). Hydrophilic residues are in blue and hydrophobic residues are in red.

(G) Same experiment as in Fig.1A with BaxWT, BaxA24R and BaxL26Q, showing the absence of precipitation of BaxA24R and BaxL26Q.

(H) Same experiment as in Fig.1C with BaxA24R showing its absence of association to nanodiscs.

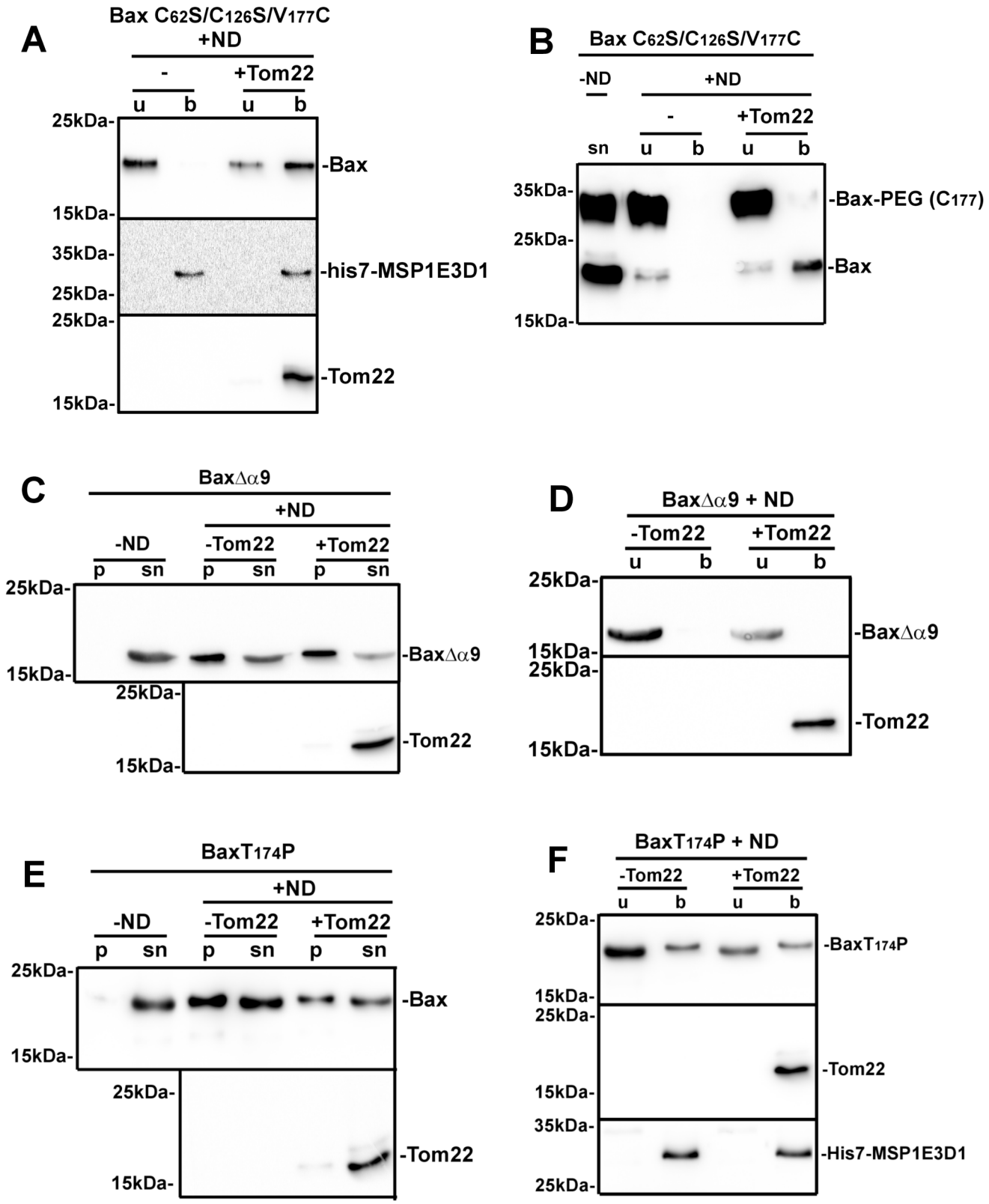
A
Bax C62S/C126S/V177C
+ND
-
+Tom22
u
b
u
b
25kDa-
-Bax
15kDa-
35kDa-
-his7-MSP1E3D1
25kDa-
25kDa-
-Tom22
15kDa-
B
Bax C62S/C126S/V177C
-ND
+ND
-
+Tom22
sn
u
b
u
b
35kDa-
-Bax-PEG (C177)
25kDa-
-Bax
15kDa-
C
BaxΔα9
+ND
-ND
-Tom22
+Tom22
p
sn
p
sn
p
sn
25kDa-
-BaxΔα9
15kDa-
25kDa-
-Tom22
15kDa-
D
BaxΔα9 + ND
-Tom22
+Tom22
u
b
u
b
25kDa-
-BaxΔα9
15kDa-
25kDa-
-Tom22
15kDa-
E
BaxT174P
+ND
-ND
-Tom22
+Tom22
p
sn
p
sn
p
sn
25kDa-
-Bax
15kDa-
25kDa-
-Tom22
15kDa-
F
BaxT174P + ND
-Tom22
+Tom22
u
b
u
b
25kDa-
-BaxT174P
15kDa-
25kDa-
-Tom22
15kDa-
35kDa-
-His7-MSP1E3D1
25kDa-

Figure 3. Effect of nanodiscs and Tom22 on the exposure and insertion of Hα9.

(A) Same experiment as in Fig.1C with the mutant BaxC62S/C126S/V177C.

(B) Fractions from **(A)** were incubated for 1 minute in the presence of 0.2mM NEM-PEG (5kDa) and the reaction was stopped by adding 20mM NEM and a 10-minutes additional incubation. The lane "-ND" is a synthesis without ND and Tom22. Samples were then analyzed by SDS-PAGE and western-blot against Bax.

(C,E) Same experiments as in Fig.1A on mutants BaxΔα9 and BaxT174P, showing that Tom22 did not prevent their precipitation.

(D,F) Same experiments as in Fig.1C on mutants BaxΔα9 and BaxT174P showing that Tom22 did not promote their insertion.

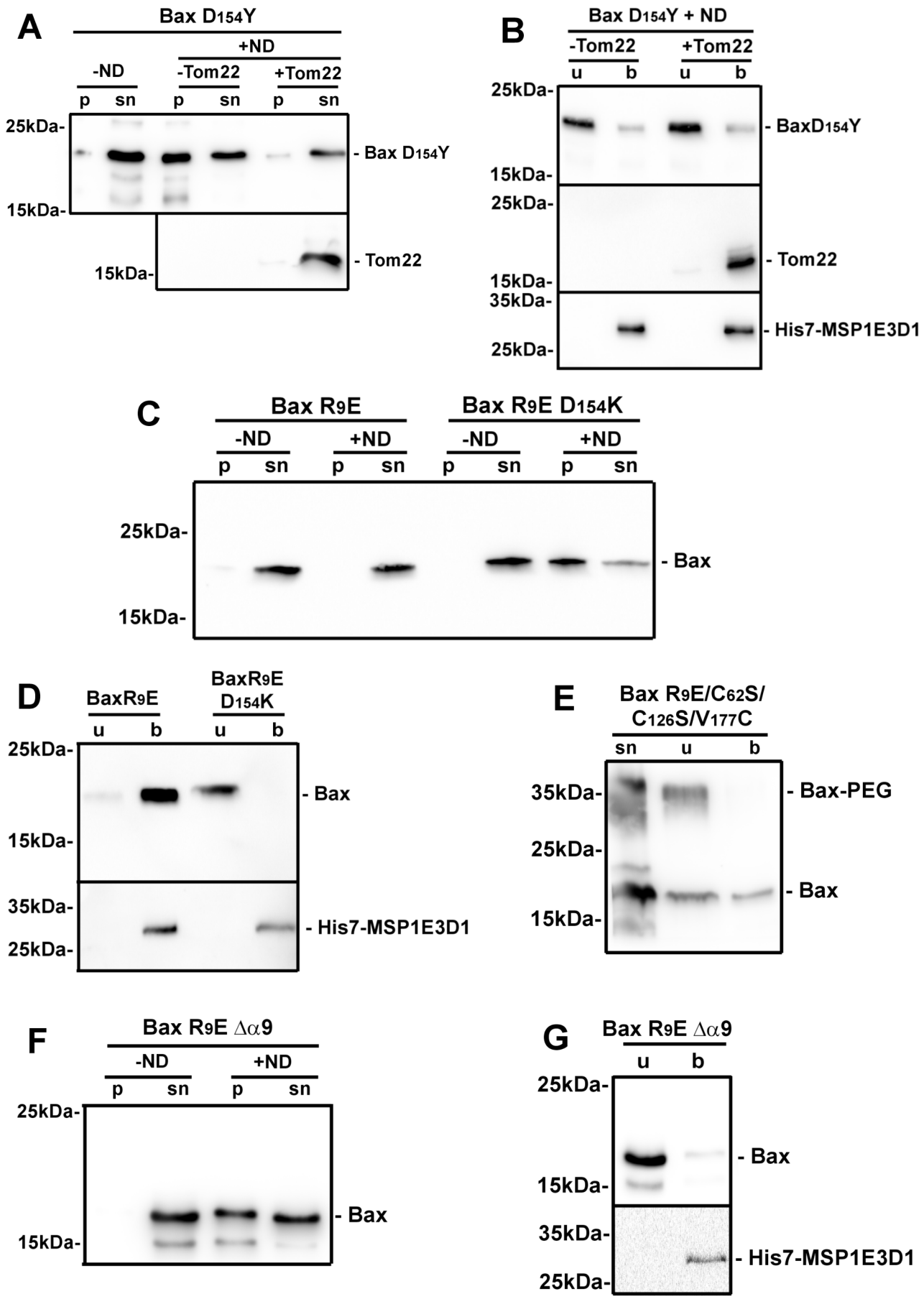
A
Bax D154Y
+ND
-ND
-Tom22
+Tom22
p
sn
p
sn
p
sn
25kDa-
15kDa-
- Bax D154Y
15kDa-
- Tom22
B
Bax D154Y + ND
-Tom22
+Tom22
u
b
u
b
25kDa-
15kDa-
- BaxD154Y
25kDa-
15kDa-
- Tom22
35kDa-
25kDa-
- His7-MSP1E3D1
C
Bax R9E
Bax R9E D154K
-ND
+ND
-ND
+ND
p
sn
p
sn
p
sn
p
sn
25kDa-
15kDa-
- Bax
D
BaxR9E
BaxR9E D154K
u
b
u
b
25kDa-
15kDa-
- Bax
35kDa-
25kDa-
- His7-MSP1E3D1
E
Bax R9E/C62S/ C126S/V177C
sn
u
b
35kDa-
25kDa-
15kDa-
- Bax-PEG
- Bax
F
Bax R9E Δα9
-ND
+ND
p
sn
p
sn
25kDa-
15kDa-
- Bax
G
Bax R9E Δα9
u
b
25kDa-
15kDa-
- Bax
35kDa-
25kDa-
- His7-MSP1E3D1

Figure 4: The R9E substitution recapitulates the effect of Tom22.

(A,B) Same experiments as in Fig.1A and 1C on mutant BaxD154Y, showing that Tom22 prevented its precipitation but did not promote its insertion.

(C,D) Same experiments as in Fig.1A and 1C on mutants BaxR9E and BaxR9E/D154K in the absence of Tom22, showing that BaxR9E was spontaneously inserted, and that the mutation D154K reversed the spontaneous insertion.

(E) Same experiment as in Fig.3B on mutant BaxR9E/C62S/C126S/V177C synthesized in the absence of Tom22, showing the spontaneous insertion of Hα9.

(F,G) The mutant BaxR9R/Δα9 was synthesized in the absence of Tom22 and analyzed as in Fig.1A and 1C, showing that the deletion of Hα9 impaired the absence of precipitation and prevented the insertion induced by the mutation R9E.

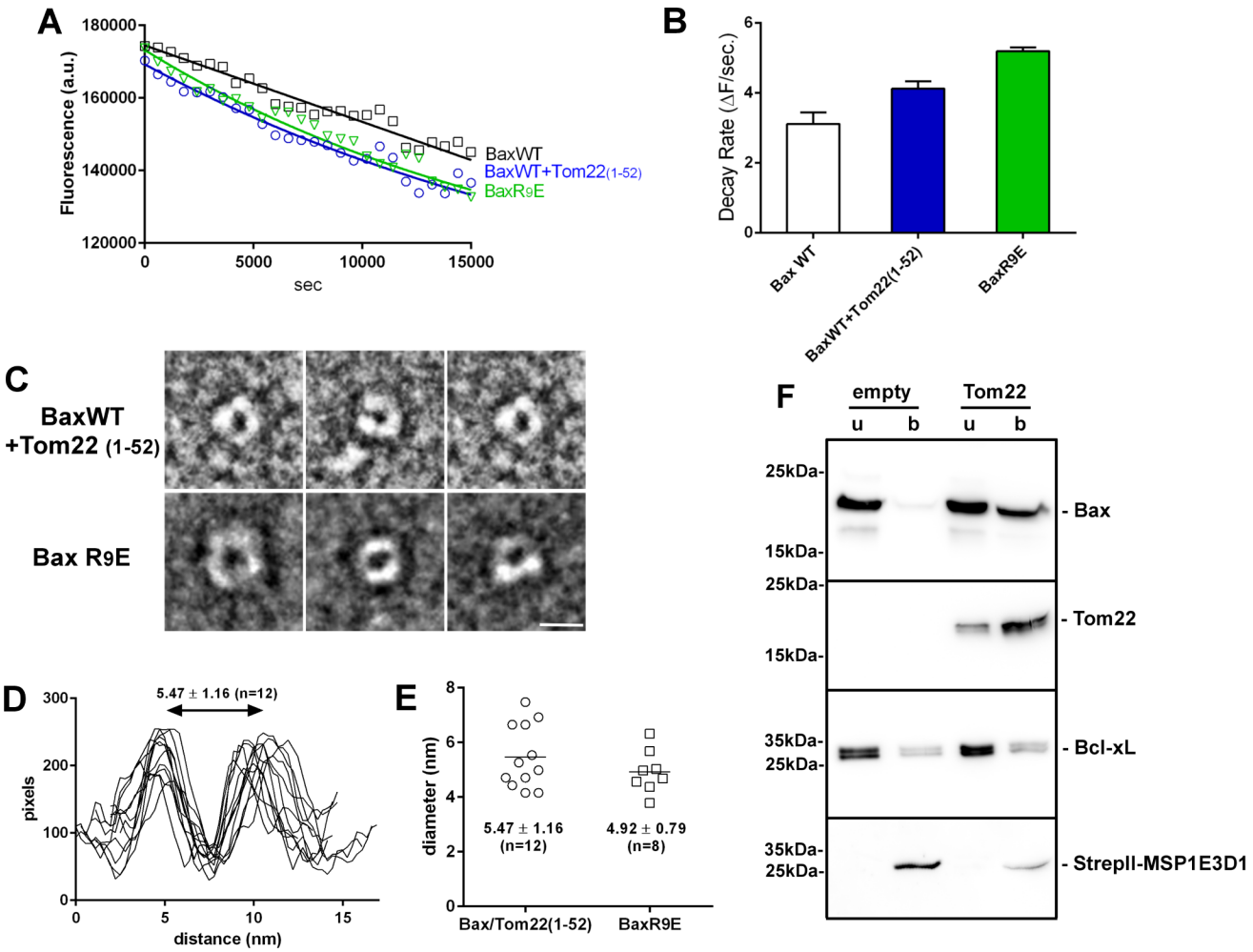

Figure 5. Effect of Tom22 and of the mutation BaxR9E on Bax biochemical properties.

(A) BaxWT was synthesized alone or co-synthesized with $Tom22_{(1-52)}$, and the mutant BaxR9E was synthesized alone. 20µL liposomes loaded with Dextran-FITC (10kDa) (Sigma) and 8µg of a fluorescence quenching anti-FITC antibody (ThermoFisher Scientific) were added in the reaction mix. Mixes were put in 96-well fluorescence plate, and incubated at 28°C in a thermostated fluorescence plate reader (Clariostar, BMG Labtech). Samples fluorescence was recorded at 10-minutes intervals (ex: 475-490 nm, em: 515-545 nm).

(B) Inital rates of fluorescence decays in experiments of **(A)**. Plots were fitted with exponential decay and the rate constants were calculated and averaged from two independent experiments. R^2 values were 0.95, 0.94 and 0.98 for BaxWT, BaxWT+$Tom22_{(1-52)}$ and BaxR9E, respectively.

(C) BaxWT was co-synthesized with $Tom22_{(1-52)}$ and BaxR9E was synthesized alone in the presence of nanodiscs. Nanodiscs were purified and concentrated on Vivaspin (cut-off 50kDa; Sartorius). They

were negatively stained with uranyle acetate and observed by TEM (see methods). Selected images showing the presence of a pore are shown. The scale bar is 10nm.

(D,E) Pixel densities were measured on images along a line crossing the largest diameter of the pores.

(F) Bax and Bcl-xL were co-synthesized in the presence of nanodiscs made with His7-tagged MSP1E3D1, purified on Ni-NTA, and dialyzed against ND buffer (200 mM NaCl, 10mM Hepes, pH 7.4) (Rouchidane Eyitayo et al., 2023b). Tom22 was synthesized in the presence of nanodiscs made with StrepII-tagged MSP1E3D1, purified on Strep-Tactin, and dialyzed against ND buffer. Bax/Bcl-xL-containing His7-nanodiscs were mixed with the same amount of StrepII-nanodiscs, either empty or containing Tom22. 250nM of WEHI-539 were added and the mixture was incubated overnight at 4°C. StrepII-nanodiscs were purified on Strep-Tactin and the unbound and bound fractions were analyzed.

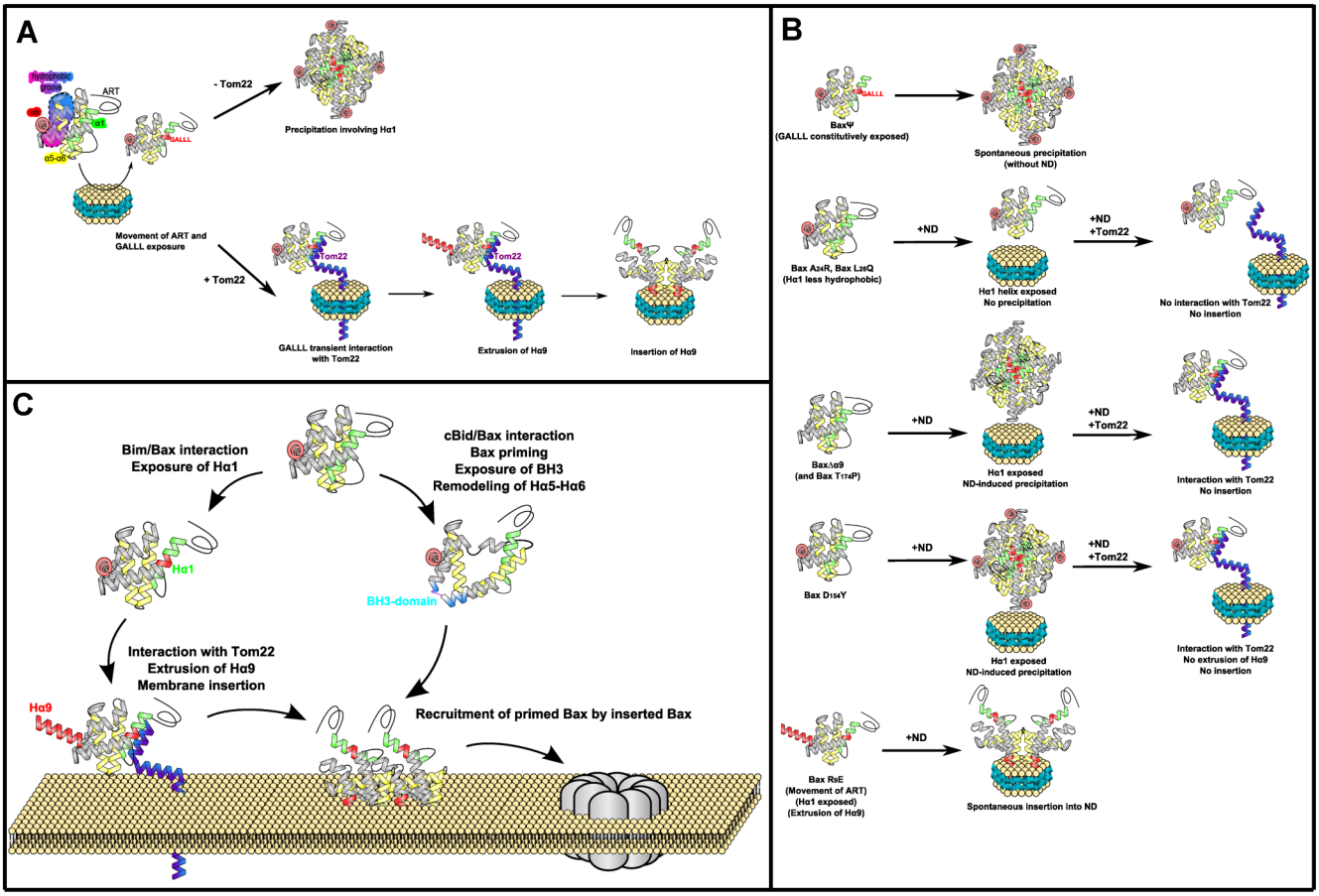

Figure 6. Representation of Bax interaction with nanodiscs and Tom22

(A) The interaction of Bax with nanodiscs induced the exposure of the GALLL motif in Hα1. In the absence of Tom22, interaction between GALLL motifs of different Bax molecules led to their precipitation. In the presence of Tom22, GALLL motif interacted with Tom22, promoting a conformationnal change leading to the extrusion, followed by the insertion of Hα9.

(B) Behavior of the different mutants investigated in this study.

- In BaxΨ, Hα1 was constitutively exposed, leading to its precipitation in the absence of nanodiscs, caused by hydrophobic interactions between GALLL motifs.

- In BaxA24R and BaxL26Q, the exposure of Hα1 did not induce Bax precipitation in the presence of nanodics; however these mutants failed to interact with Tom22 and therefore were not inserted.

- Like BaxWT, the mutants BaxΔα9 and BaxT174P expose the GALLL motif in the presence of nanodiscs, and interact with Tom22. However, in the absence of an adequate Hα9, they are not inserted into nanodiscs

- The mutant D154Y, like BaxWT, was precipitated in the presence of nanodiscs, and could interact with Tom22; however, it did not support the conformational change leading to Bax insertion.
- The interaction of mutant R9E with nanodiscs led to the conformational change leading to the extrusion and insertion of Hα9 even in the absence of Tom22.

(C) Hypothetic model of the concerted involvement of BH3-only proteins and Tom22 in Bax insertion in the MOM. The interaction of Bim with Bax at the non-canonical binding site induces the exposure of the Hα1, allowing the interaction of Bax with Tom22. Bax/Tom22 interaction leads to the extrusion and insertion of Hα9, associated to the exposure of the BH3-domain. The interaction of cBid with Bax induces the exposure of the BH3-domain and the remodeling of the Hα5/Hα6 (Czabotar et al., 2013), allowing the recruitment of cBid-activated Bax by membrane-inserted Bax, leading to the formation of membrane oligomers.

Supplementary data

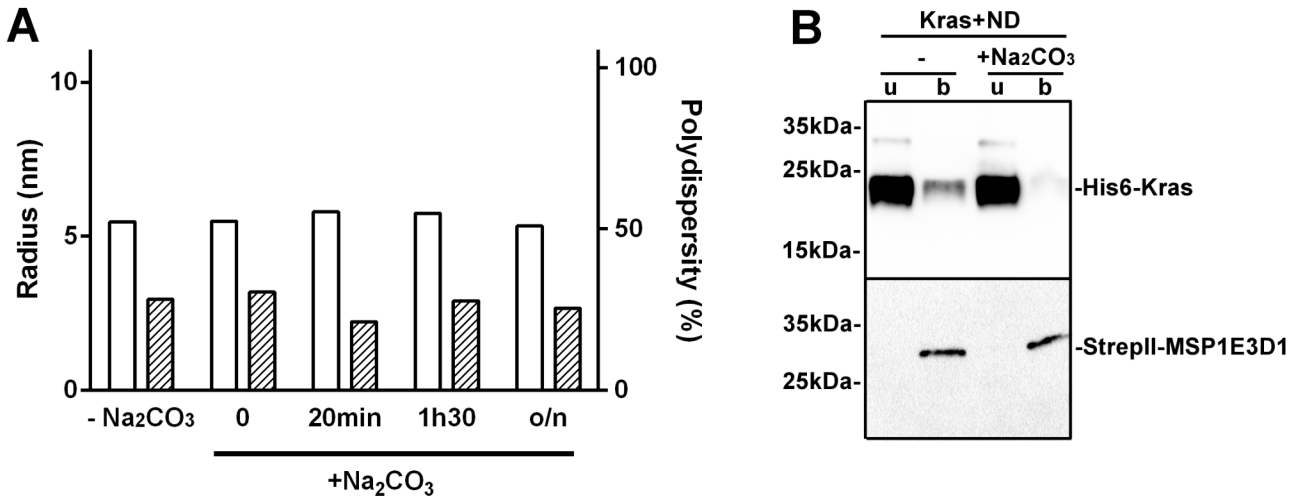

Figure S1. Controls of the effect of alkaline Sodium Carbonate treatment on nanodiscs.

(A) Nanodiscs were incubated for the indicated times in the presence of 0.1M Sodium Carbonate (pH 10.0). Radius and polydispersity were measured by DLS (3 measurements of 10 acquisitions each), showing that the integrity of nanodiscs was not affected by the treatment.

(B) His6-tagged human Kras was synthesized in cell-free in the presence of StrepII-MSP1E3D1 nanodiscs. Nanodiscs were purified on StrepII-Tactin, then incubated for 10 minutes in the absence or in the presence of 0.1M Sodium Carbonate (pH 10.0). They were then re-purified on StrepII-Tactin, and the unbound and bound fractions were analyzed by western-blots. A minor fraction of Kras remained bound to nanodiscs, but was removed after alkaline treatment.

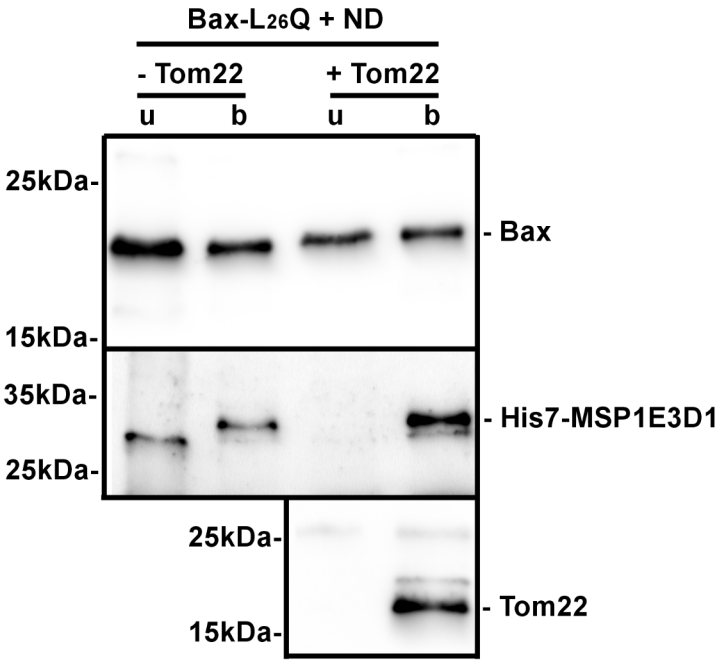

Fig.S2: The mutation L26Q in the GALLL motif partially abolishes Tom22-induced Bax insertion.

Same experiment as in Fig.2H with BaxL26Q instead of BaxA24R.

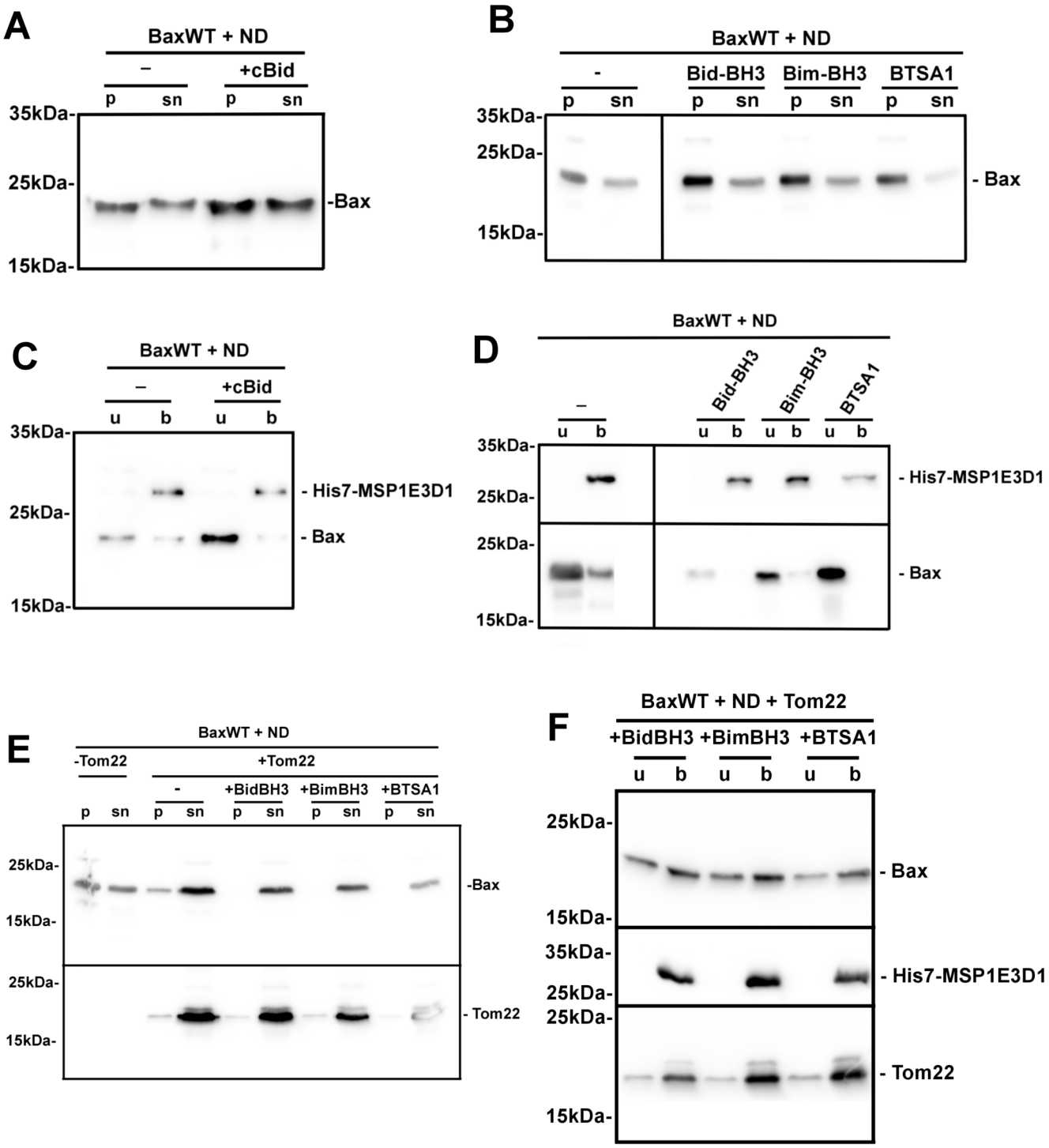

Figure S3. BH3-activators do not prevent Bax precipitation nor promote Bax insertion into nanodiscs

(A,B) Same experiments as in Fig.1A and 1C (without Tom22), except that 10µg caspase-8-cleaved Bid (cBid) was included in the reaction mix. We determined that the typical concentration of Bax produced in the cell-free system was 0.5 mg/mL, *i.e.* 50µg of Bax in the 100µL-reaction mix. We therefore set up a cBid to Bax ratio of ~1 to 5 (considering that the sizes of the two proteins are close to each other) (Shamas-Din et al., 2015).

(C,D) Same experiment as in Fig.1A and 1C (without Tom22) in the presence of 1µM Bim-BH3 (PEIWIAQELRRIGDEFNAYYA) Bid-BH3 (ESQEDIIRNIARHLAQVGDSMDRSIPPG), or BTSA1 (Medchem). The concentration refers to the whole mix (reaction mix + feeding mix) because the sizes of the three molecules are below the cut-off of the dialysis membrane.

(E,F) Same experiments as in **(C,D)** in the presence of Tom22.

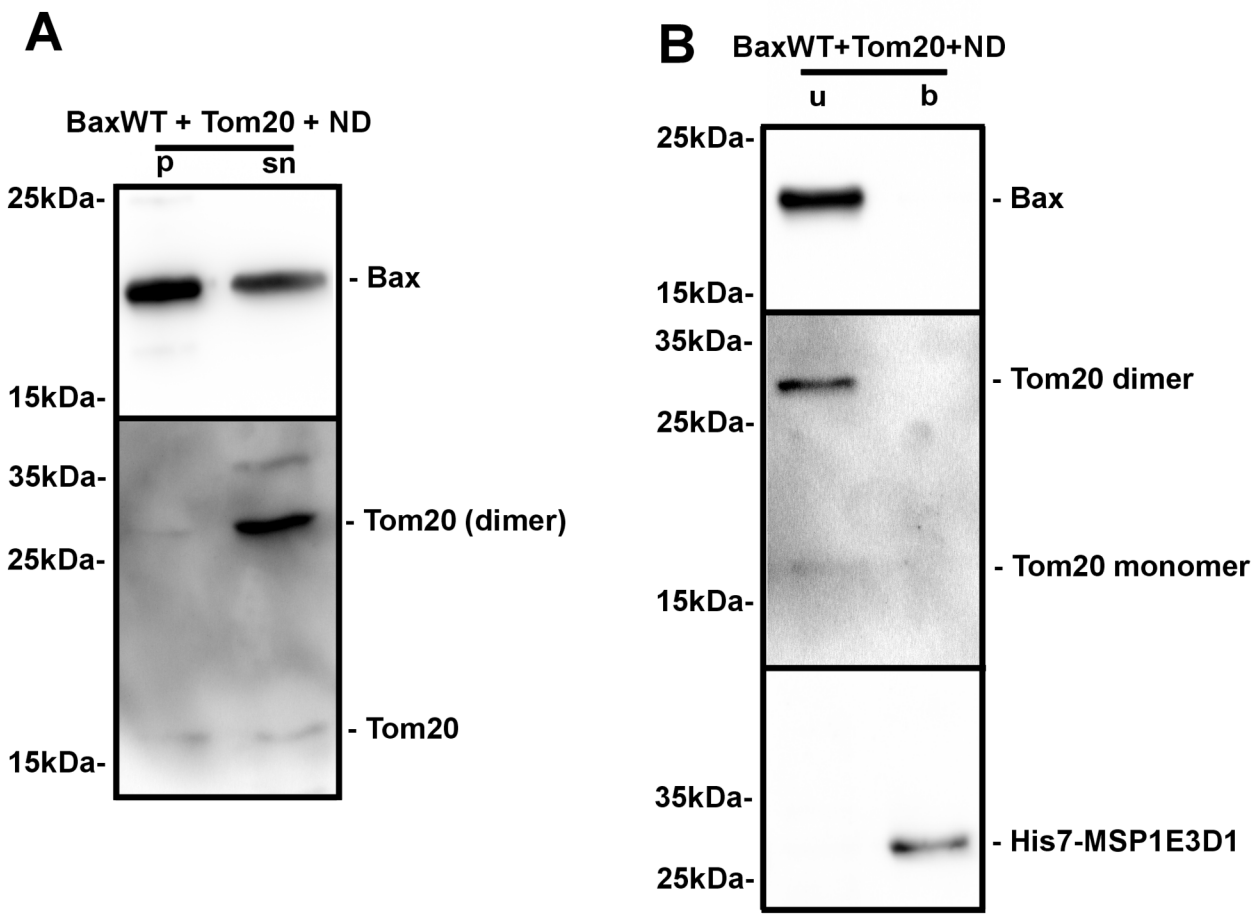

Figure S4. Specificity of the effect of Tom22.

(A,B) Bax was synthesized alone or co-synthesized with Tom20 and analyzed as in Fig.1A and 1C showing that Tom20 did not prevent Bax precipitation and did not promote its insertion.

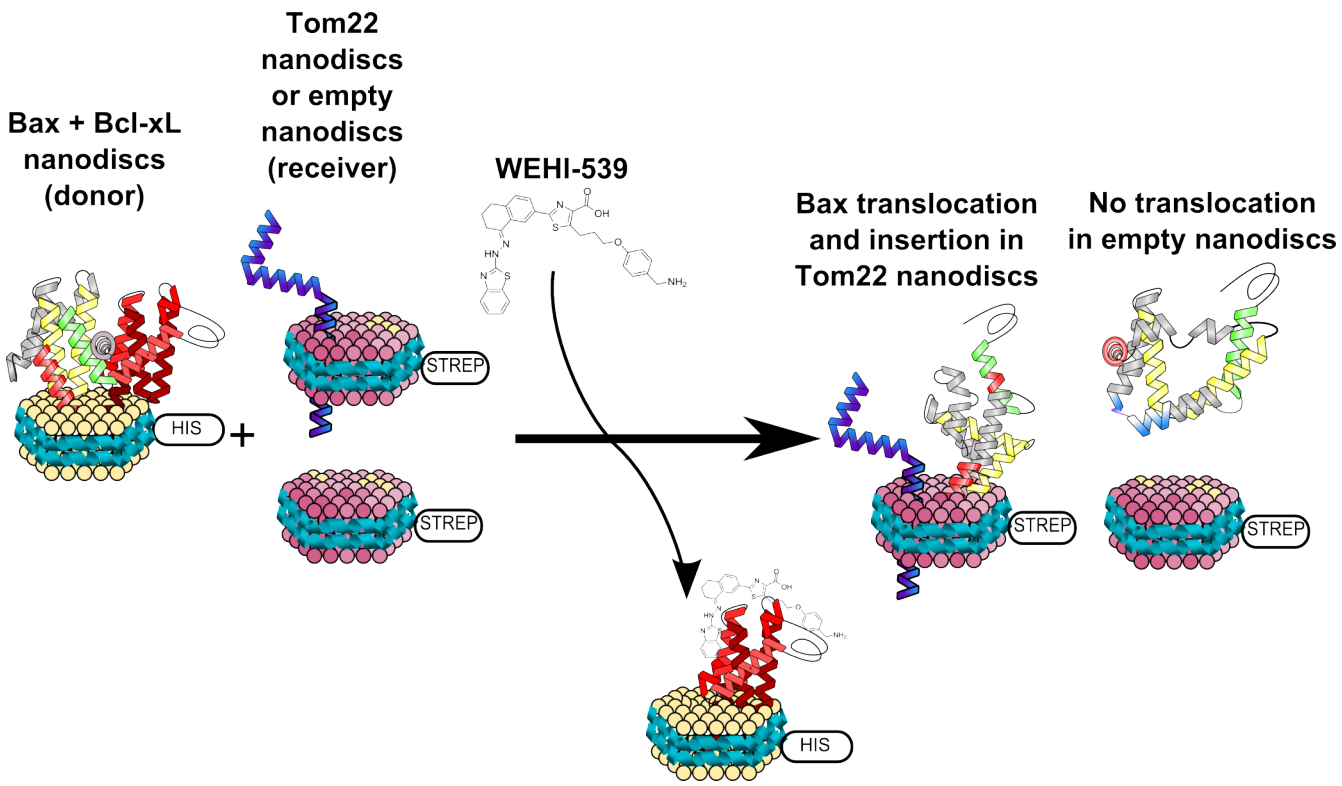

Figure S5: Representation of the role of Tom22 in Bax translocation from an inactive dimer with Bcl-xL to a self-inserted conformation

The addition of WEHI-539 to Bax/Bcl-xL heterodimers inserted in nanodiscs releases Bax under a primed conformation (Gautier et al., 2011) followed by its membrane insertion into nanodiscs only when Tom22 is present.

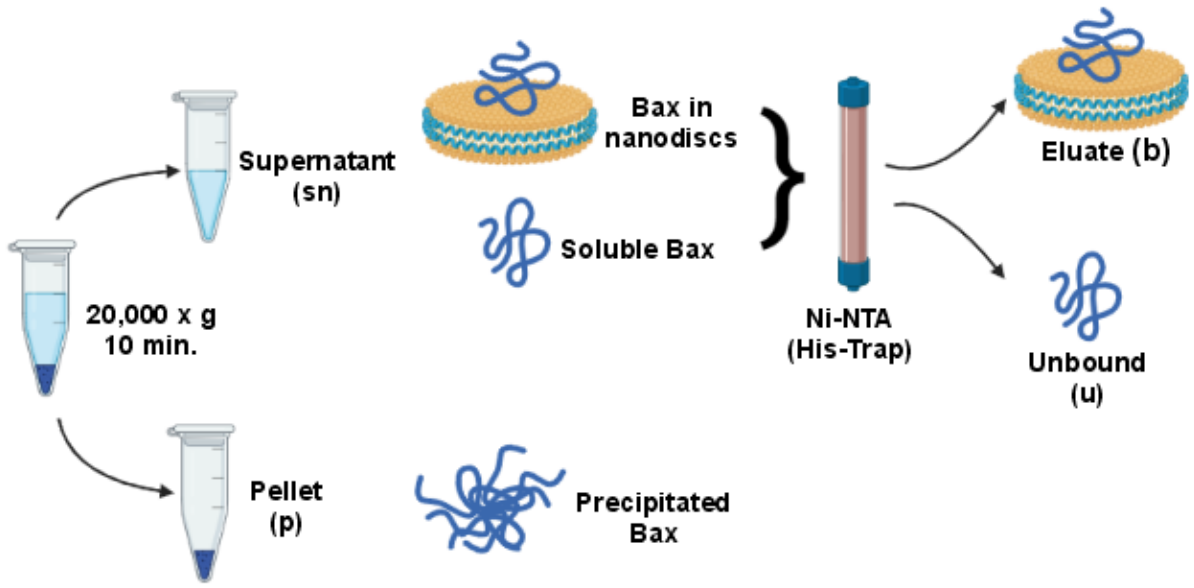

Figure S6. Schematic representation of the experimental flow.

After cell-free synthesis, a 15-minutes, 20,000 x g centrifugation led to a pellet (p) of precipitated proteins and a supernatant (sn) containing soluble Bax and nanodiscs (empty or with inserted Bax). The supernatant was loaded on Ni-NTA (His-Trap). The flow-through contained soluble Bax unbound to nanodiscs (u). After an elution with 300mM imidazole, the eluate contained nanodiscs (empty or with inserted Bax) (b).

Table S7: antibodies used in this study

Bax	sc-20067, 2D2, Santa-Cruz Biotechnology	Mouse monoclonal	1:5000 PBST/milk
Bax	sc-23559, 6A7, Santa-Cruz Biotechnology	Mouse monoclonal	IP (1µg)
Bax	ab182734, Abcam	Rabbit monoclonal	1:10000 TBST/milk
Tom22	ab179826, Abcam	Rabbit monoclonal	1:5000 TBST/milk
Tom20	ab186735, Abcam	Rabbit monoclonal	1:5000 TBST/milk
His6 tag	ma1-135, ThermoFisher Scientific	Mouse monoclonal	1:10000 PBST/milk
HA tag	71-5500, ThermoFisher Scientific	Rabbit polyclonal	1:10000 PBST/milk
StrepII tag	2-1507-001, IBA Life Sciences	Mouse monoclonal	1:5000 PBST/milk
FITC	701078, ThermoFisher Scientific	Rabbit monoclonal	Quenching (4µg)
Bcl-xL	E18, ab32370, Abcam	Rabbit monoclonal	1:10000 TBST/milk